(1)

24(1)

気象庁欧文海洋報告

第24巻 第1号

THE OCEANOGRAPHICAL MAGAZINE

LIBRARY
APR 2 1973
FISH & WILDLIFE SERVICE

Vol. 24 No. 1

CONTENTS

MORIYASU, S.: On short-term fluctuations of the Tsushima Current to the northwest of the Noto Peninsula in October 1969 1

NAGASAKA, K. and T. SAWARA: A preliminary report of the cruise of the R/V *Ryofu Maru* in January-March 1971 25

IIDA, H.: Edge waves on the linearly sloping coast II. Forced waves and β-effect 39

AKAGAWA, M.: The mean sea surface temperature of the Okhotsk Sea in cooling season (Second report) ——Normal sea surface temperature—— .. 57

YOSHIMURA, H.: On the distribution of phosphorus along 170°W longitude in the Pacific and Antarctic Oceans 65

Published by the Japan Meteorological Agency

December, 1972

The Oceanographical Magazine
Vol. 24, No. 1, pp. 1 to 23, December 1972

On short-term fluctuations of the Tsushima Current to the northwest of the Noto Peninsula in October 1969

Shigeo MORIYASU

Meteorological Research Institute

(Received September 7, 1972)

Abstract; This is a report on the observation on short-term fluctuation of the Tsushima Current in October 1969. This observation consists of repeated observations on a fixed line and at fixed stations. Though the period of the observation is short and strict discussions are impossible, general features of short-term fluctuations are given for temperature, current velocity and so on. In addition, discussions are made on the relation in variations between temperature and current velocity.

1. Introduction

A cooperative observation of the Japan Sea was planned by the Marine Division of the Japan Meteorological Agency, and five vessels of the Japan Meteorological Agency and four marine observatories took part in the observation in October 1969. The observation consists of two parts. The one is the hydrographic observation covering the whole area of the Japan Sea and the other is the observation of the short-term variation in the hydrography in the sea northwest of the Noto Peninsula. The present report deals with the results of the latter observation.

This observation was planned to study the short-term variation of the Tsushima Current and of the cold water region in the sea northwest of the Noto Peninsula. At the time of the observation, however, there was no cold water region, but a warm water region was seen. Then, we changed the object of study to this warm water region.

Preliminary observation was carried out on 19 October to see the details of the hydrography in the considered region and to make the final plan of the main observation. The observation was completed by the participation of four research vessels, *Seifu Maru, Kofu Maru, Chofu Maru* and *Shumpu Maru.*

The main observation was carried out from 25 October to 1 November. Hydrographic observations along a fixed line were repeated, and BT observations and direct current measurements were made at fixed stations. Besides the four vessels

noted above, R/V *Ryofu Maru* participated in this observation. Completion of the plan was prevented by rough weather and amount of data obtained was below that of expected.

2. Preliminary observation

Four hydrographic sections were completed with BT observations down to 250 m depth. In addition, surface current measurements were made with GEK. The location of sections is shown in Fig. 1. Twelve hydrographic stations were distributed at an interval of 10 nautical miles on each section. One section was assigned to each vessel and the observation started at the southernmost station of the section at 09 LST on 19 October and was finished at the northernmost station of the section before midnight of the day. Simultaneous observation was planned to remove the effects of diurnal variations for the close network.

Fig. 1 shows the distribution of water temperature at 100 m depth and surface current. There is a warm water region the center of which is located at 38°40′N, 135°50′E. The region is accompanied with an anticyclonic eddy and the Tsushima

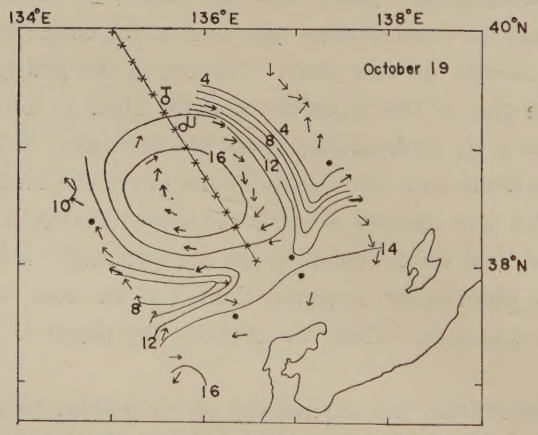

Fig. 1. Temperature (°C) at 100 m depth and surface current measured with GEK in preliminary observation.
Surface current
●: less than or equal to 0.2 knot
←: greater than 0.2 knot and less than 1.0 knot
←: equal to or greater than 1.0 knot
×: station on the fixed line in main observation
○: fixed station in main observation

Current meanders around the region. Since the observation did not cover the whole area of the warm water region, dimensions of the warm water region and of the meandering cannot be determined. Probably, the amplitude of the meandering is more than 50 nautical miles.

Based on the results of the observation, a fixed line and a fixed station, Station T in Fig. 1, were selected for the main observation.

3. Repeated hydrographic observation along the fixed line

Hydrographic section was made along the fixed line, on which fifteen stations were distributed at an interval of 10 nautical miles. The plan was as follows:

1) The section is made once a day.
2) Obsevation of the section starts at St. 1 (the southernmost station) at 18 LST of the first day and ends at St. 15 (the northernmost station) in the evening of the second day.

But, the operation was interrupted by rough weather and only six sections were

Table 1. Itinerary of repeated observation.

Section	Date	Vessel	Stations occupied
I	Oct. 25—26	*Seifu Maru*	1—15
II	Oct. 26—27	*Kofu Maru*	1—12
III	Oct. 28—29	*Ryofu Maru*	4—12
IV	Oct. 29—30	*Chofu Maru*	1—15
V	Oct. 30—31	*Shumpu Maru*	1—15
VI	Oct. 31	*Chofu Maru*	1— 5
	Nov. 1	*Ryofu Maru*	6—15

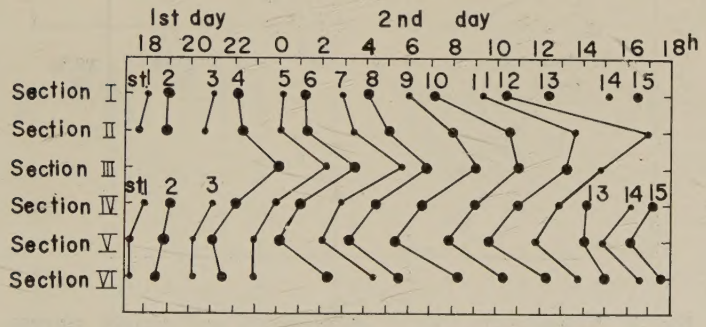

Fig. 2. Record of operation of repeated observation.
small dot: BT and GEK observations
large dot: BT, GEK and serial observations

obtained (Table 1). Two sections, Section II and Section III, are not complete. Time interval of observations at individual stations is expected to be 24 hours, but the interval is much deviated from 24 hours (Fig. 2) and so diurnal variation is not

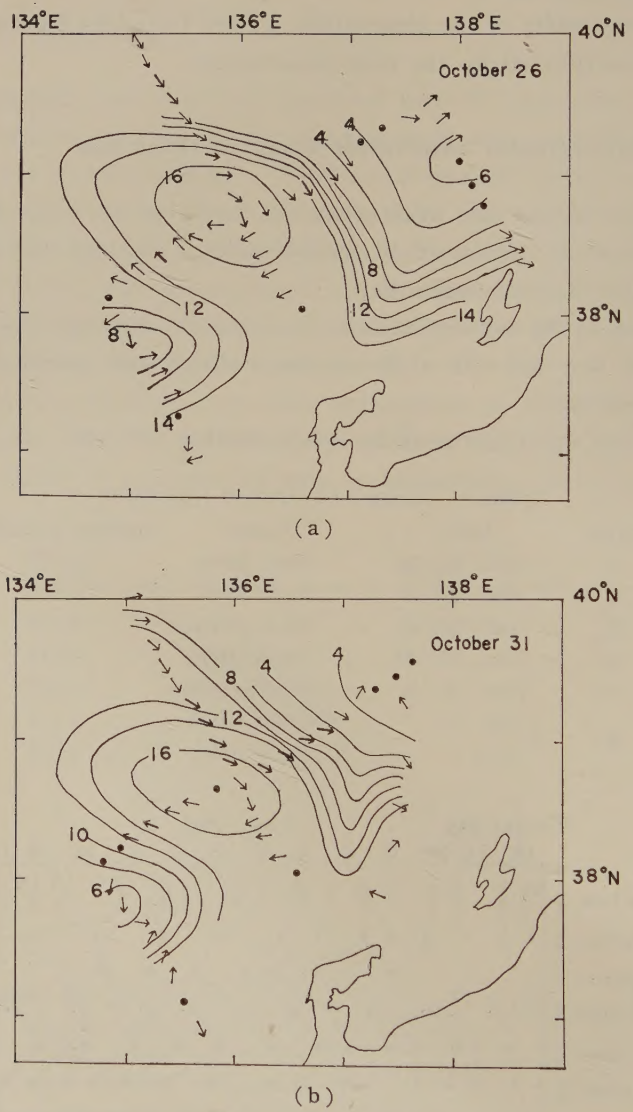

Fig. 3. Temperature (°C) at 100 m depth and surface current measured with GEK (a) at the beginning and (b) at the end of main observation. Surface current is shown by the same symbols as those used in Fig. 1.

removed for some stations. As the section is set up through the warm water region and across the Tsushima Current, day-to-day variation of the Tsushima Current and the warm water region must be caught by repeated observations.

Subsidiary observations were made with BT and GEK at the beginning and the end of the main observation (Fig. 3). According to the results, the hydrographic pattern was nearly the same, and marked variation was found neither in the

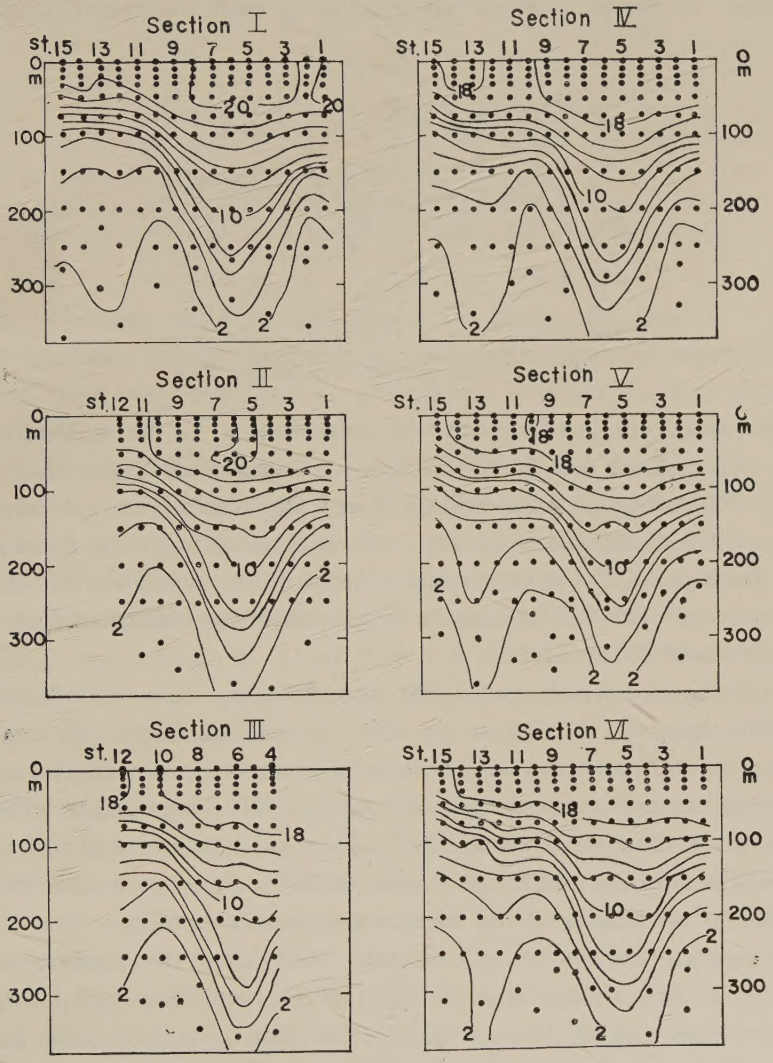

Fig. 4. Temperature sections (°C).

Tsushima Current nor in the warm water region during this period. Therefore, fluctuation described below is an example under stable hydrographic conditions.

Temperature sections are shown in Fig. 4. It is also inferred from the figure that there is no marked variation in the distribution of temperature. Temperature is higher than 18°C in the upper mixed layer of thickness of 50–75 m and decreases markedly to 2~4°C in the thermocline. The Tsushima Current is between St. 7 and St. 10 and the center of the warm water region is around St. 5. These features are common to the six sections and are clear in mean distribution (Fig. 5). The

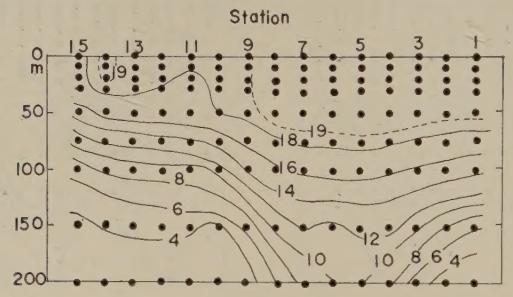

Fig. 5. Mean temperature section (°C).

observation was made in the season when temperature in the surface layer falls and the mixing layer increases in thickness. Temperature higher than 20°C was measured only in Section I and Section II, but the thickness of the mixing layer had not a trend of increase in general. An interesting feature is found at Sts. 12 and 13. Isotherm of 2°C is deeper and a warm water extends down to 300 m depth at these stations. This is inferred to be brought about by sinking, but such a feature is not seen above 200 m depth.

T-S relationships remain unchanged throughout the main observation, and the intermediate water and the Chukan-sui water are distinguished in the relationships. Therefore, the distribution of salinity is almost completely dependent upon temperature. Gross features are common to all sections. The intermediate water of high salinity is at 70–150 m depth of Sts. 4–8 and its thermosteric anomaly is 200–300 cl/ton. A water of high salinity goes down to 300 m depth at St. 13. This feature corresponds to the sinking of the warm water mentioned before. The Chukan-sui water is characterized by salinity of about 34.05‰ and thermosteric anomaly of about 75 cl/ton, and is found at depth equal to or greater than 300 m. At St. 10, both temperatures and salinities are lower below 150 m depth and salinity corresponding to a temperature is a little lower than salinity around the station. This is

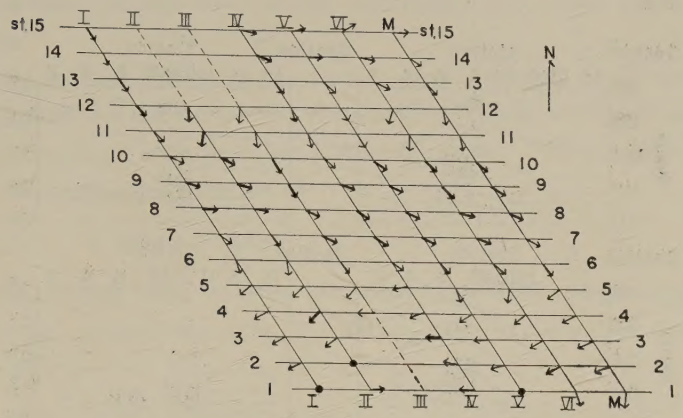

Fig. 6. Surface current measured with GEK.
Arabic numerals are section number and "M" means mean current.
Surface current is shown by the same symbols as those used in Fig. 1.

inferred to be brought about by upwelling of the Chukan-sui water.

Fig. 6 illustrates the distribution of surface currents measured with GEK in each section and their mean distribution. The section is in the direction of 327° true from the north and is not perpendicular to the strong current of the Tsushima Current against the expectation. In mean conditions, the stream axis is at St. 8 and the center of the warm water region is between St. 5 and St. 6. The position of the stream axis depends upon section and is between St. 7 and St. 10. The stream axis has a trend to move southward about 20–30 nautical miles in a week. And, the center of the warm water region is between St. 6 and St. 7 in Section I and Section II and between St. 5 and St. 6 in other sections. Thus, it is inferred that both the stream axis and the center of the warm water region are shifted southward in the main observation.

Geostrophic current speeds perpendicular to the section are computed on the basis of hydrographic casts. Distance between the stations is 10 or 20 nautical miles and the reference level is 300 db surface. Dynamic depth anomalies of some isobaric surfaces are shown in Fig. 7. The features in Fig. 6 are also clear in this figure. At 200 db surface, speeds higher than 10 cm/sec are obtained. The position of the stream axis of the Tsushima Current at the surface is nearly the same as the position estimated from GEK observations, while the axis is deviated slightly southward at 150 m or 200 m depth. A clockwise eddy around the warm water region is ascertained by the distribution of geostrophic current, too. North of the axis, there

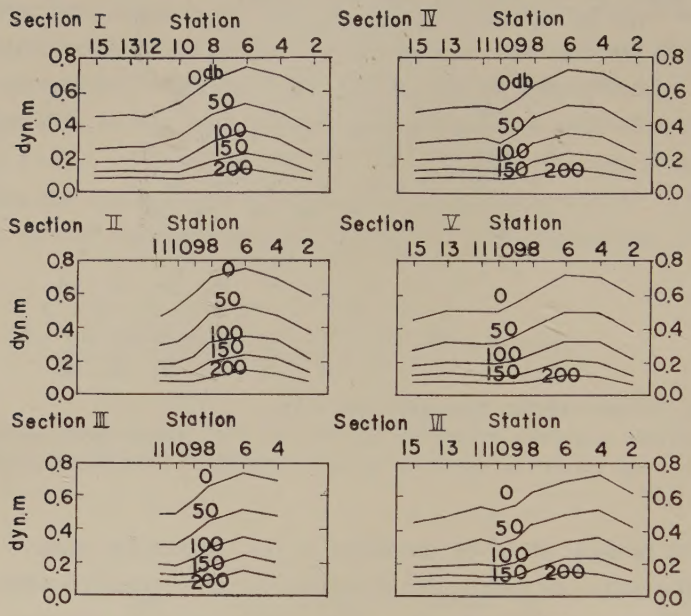

Fig. 7. Form of isobaric surfaces referred to 300 db surface.

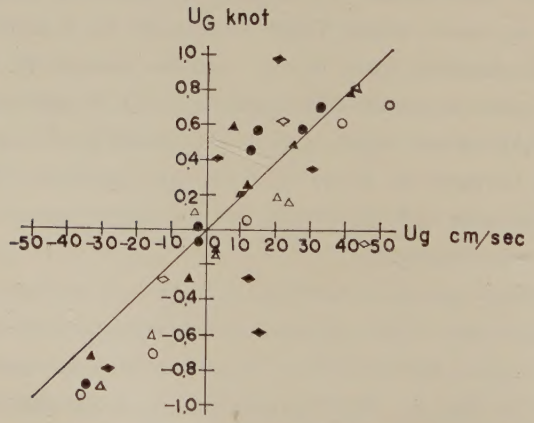

Fig. 8. Comparison of NE-component between geostrophic current and current measured with GEK.
U_g: geostrophic current at the surface referred to 300 db surface
U_G: surface current measured with GEK
△: Section I ○: Section II ◇ Section III
▲: Section IV ●: Section V ◆ Section VI

is a narrow counter current down to the reference level. These features are found in all sections.

Geostrophic current speeds at the surface are compared with current speeds measured with GEK for the component perpendicular to the section (this component is called NE-component and the other NW-component). The correlation coefficient is 0.805 and the regression equation is

$$U_G = -0.1069 + 0.0193 U_g .$$

U_G and U_g are current speed in knot measured with GEK and geostrophic current speed in cm/sec, respectively (Fig. 8). When U_G is expressed in cm/sec, the regression equation is

$$U_G = -5.59 + 0.9920 U_g$$

and geostrophic current is slightly higher. Thus, a reasonable linear relation is found though the deviations from the relation are large for some samples. This means that the selection of the reference surface is appropriate in the computation of geostrophic current speed.

Mean value of the geostrophic current speed from the surface to 300 db surface

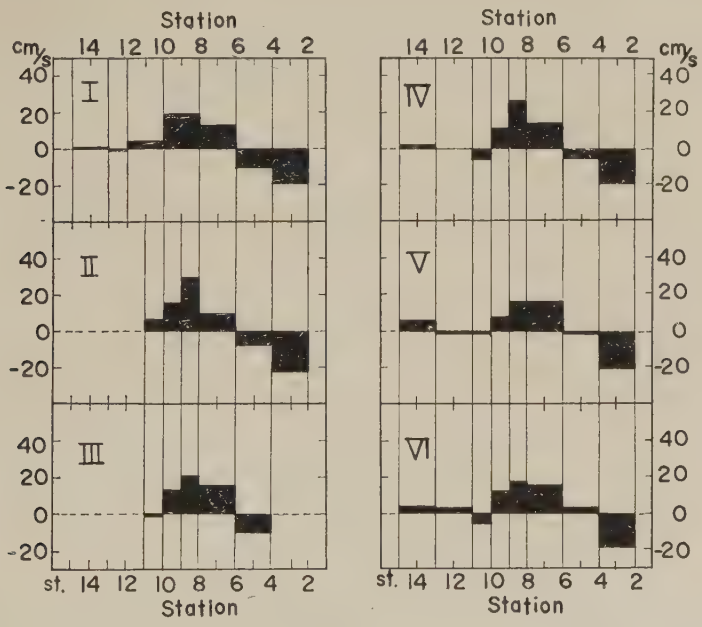

Fig. 9. Mean geostrophic speed from the surface to 300 db surface. Arabic numerals are section number. Positive sign means NE-ward speed.

is also computed for each section (Fig. 9). Since Sections II and III are not complete and the distance between adjacent stations are not common, the distribution of the mean speed cannot be compared between sections in strict sense. The high speed zone and the anticyclonic eddy, however, are found in the position mentioned above.

From the distribution of mean speed, volume transport perpendicular to the section is estimated. The estimate is made on the assumptions that northeastward current is composed of the Tsushima Current and the anticyclonic eddy and that the southwestward current at Sts. 2–6 is due to the eddy. Then, net volnme transport of the Tsushima Current is expressed as their difference (Table 2). The value of

Table 2. Volume transport (10^6 m^3/sec) perpendicular to the section referred to 300 db surface.

Section	Total (1)	Eddy (2)	Difference (1)–(2)
I	4.15	3.21	0.94
II	4.05	3.13	0.92
IV	3.78	2.71	1.07
V	3.37	2.43	0.94
VI	3.52	2.34	1.18

volume transport computed in this way has some uncertainty, but significant com parison can be made of the value obtained in a same way. St. 2 is close to the edge of the eddy in all the section and the volume transport outside this station is supposed to be small so that the value given here is nearly true one. The volume transport of the Tsushima Current has a trend of increase, $0.031 \times 10^6 m^3$/sec/day, that is, the value at the end of the main observation is 1.26 times the initial value, while the volume transport of the eddy decreases at the rate of $0.177 \times 10^6 m^3$/sec/day and the volume transport at the end is 0.73 times the initial value.

The assumption means that the volume transport of the Tsushima Current is independent of the volume transport of the eddy. Then, the two volume transports present a trend opposite to each other. The feature is expected to be sure even if the uncertainty of the computation is taken into account. It is doubtful if this interesting feature is always found. The volume transport of the eddy is much larger than the Tsushima Current's. The former is $2.34–3.21 \times 10^6 m^3$/sec, while the latter is $0.94–1.18 \times 10^6 m^3$/sec. According to YI's computation (1966) referred to 125 db surfaces, $1.35 \times 10^6 m^3$/sec of water is supplied to the Japan Sea through the Tsushima Strait. The value obtained here is close to his value.

As stated before, gross hydrographic pattern was kept unchanged during the main observation. The warm water region is found in all the section. Fluctuations

of its position and dimension in the section are not marked, and their fluctuation in the direction perpendicular to the section is not examined. Usually, temperature at 200 m depth is taken as an index of the warm water region. The highest temperature measured at 200 m depth in the region fluctuated with a range of 0.4°C and characteristic feature is not found in the fluctuation based on six samples. There is not marked fluctuation in length of section of temperature higher than 8°C at 200 m depth (Fig. 4). Slight variability of these two elements means that the warm

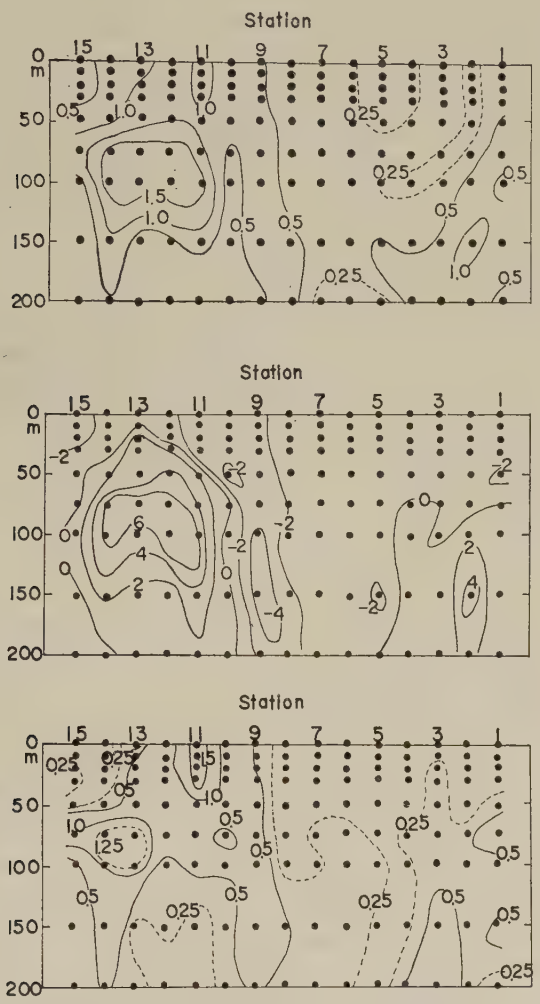

Fig. 10. Sections of indexes indicating extent of fluctuation of temperature.
upper: σ in °C middle: a in 10^{-1} °C/day lower: σ_1 in °C

water region was kept in stable conditions during the 7 days. Detailed examination will show variations of smaller scale, but available data are not fit for such examination. Volume transport by the eddy decreased and the dimension of the region was not changed. This leads to decrease of current velocity in the region, because the decrease of volume transport by the eddy is significant. Thus, decay of the eddy may be derived from these situations or the 7 days are inferred to be in the stage of decrease in the long-term fluctuation of intensity of the eddy.

In the above descriptions, mean conditions and rough features in fluctuations are presented. Though the data are not enough to examine fluctuations in detail, fluctuations of temperature and surface current are studied on an assumption.

Fig. 10 shows the distribution of standard deviation of temperature at standard depth. The value less than 0.5°C is predominant and the value greater than 1.5°C is found at 75 m and 100 m depths of Sts. 11–13, where temperature has a marked trend of increase by about 4°C in a week. At the stream axis of the Tsushima Current and in the warm water region, standard deviations are not so large. This is taken as an example of the fluctuation under stable hydrographic conditions. Though a marked variation was not found in the stream axis of the Tsushima Curernt and in the warm water region, a distinguished trend appeared in other area.

Fig. 10 also shows trend of temperature, which is computed by the method of least squares on the assumption that variation of temperature is linear with time. The greatest magnitude amounts to 0.70°C/day or more and the trend is large where standard deviation is large. This means that large standard deviation is

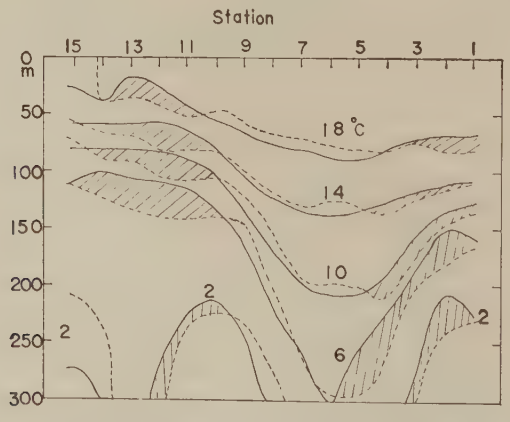

Fig. 11. Variation of depth of isotherms between Section I (full line) and Section VI (broken line).
Shaded portion means increase of the depth.

caused by linear variation. Marked trend of increase is found around 100 m depth of Sts. 11–13 and at 150 m depth of St. 2, and trend of decrease around 100 m depth of St. 9. Trend of decrease is found in the upper layer at all the station. This results from seasonal change, cooling at the surface. Vertical section of the trend proves southeastward movement of the stream axis and of the warm water region, and invasion of warm water in the northern part of the section. The invasion of warm water around St. 12 is expected to be caused by sinking. The comparison of temperature sections (Fig. 11) may serve illustration of the mechanism.

In such a treatment, temperature at time t_i is expressed by

$$y_i = y_1 + at_i + z_i ,$$

where a is a constant indicating degree of trend and z_i is deviation from the linear variation. And the following assumptions are made:

$$t_i < t_{i+1} , \quad i = 1, 2, \ldots , n$$
$$t_1 = 0 ,$$
$$z_1 = 0 .$$

This means that the trend is defined as the increase or decrease referring to y_1. Then, standard deviation is given by a equation

$$\sigma^2 = \frac{1}{n}\left(\sum_{i=1}^{n} y_i^2 - n y_0^2 \right)$$
$$= -(y_1 - y_0)^2 + \frac{a^2}{n} \sum_{i=1}^{n} t_i^2 + \frac{2a}{n} \sum_{i=1}^{n} t_i z_i + \sigma_1^2 ,$$

where

$$y_0 = \frac{1}{n} \sum_{i=1}^{n} y_i ,$$
$$\sigma_1^2 = \frac{1}{n} \sum_{i=1}^{n} z_i^2 ,$$

that is, σ_1 is the root mean square of the deviation from the linear variation. This relation indicates that variance σ^2 is dependent on σ_1^2 and a^2. If the variation is completely linear with time, z_i vanishes and σ^2 is determined by a alone. On the other hand, if the trend is not found, σ_1^2 is larger by $(y_1 - y_0)^2$ than σ^2. Though it is not clear which is more important, both σ_1^2 and a contribute to σ^2. Vertical section of σ_1 is shown in Fig. 10. Large vslues of σ_1 is found where standard deviation is large as magnitude of the trend is. Sampling interval is one day and the scale smaller than 2 days is beyond our scope. And time interval between the

first and the last samples is about 7 days. Thus, variation of a period longer than 2 days is estimated on the basis of variation of z_t. Zero-up or zero-down method gives the period, but it is difficult what period is predominant. The trend is obtained from the variation in 7 days. Therefore, a may be roughly interpreted as magnitude of variation of a period of about 2 weeks or more. σ^2 is expressed by a linear

Table 3. Correlation coefficients of σ_1^2 and a^2 with σ^2.

	Temperature									Surface current	
	0^m	10^m	20^m	30^m	50^m	75^m	100^m	150^m	200^m	NE-comp.	NW-comp.
σ_1^2	0.852	0.855	0.831	0.915	0.887	0.832	0.639*	0.421*	0.671	0.733	0.123*
a^2	0.912	0.913	0.939	0.953	0.911	0.959	0.955	0.890	0.536*	0.791	0.850

Values with * are less than 1% point.

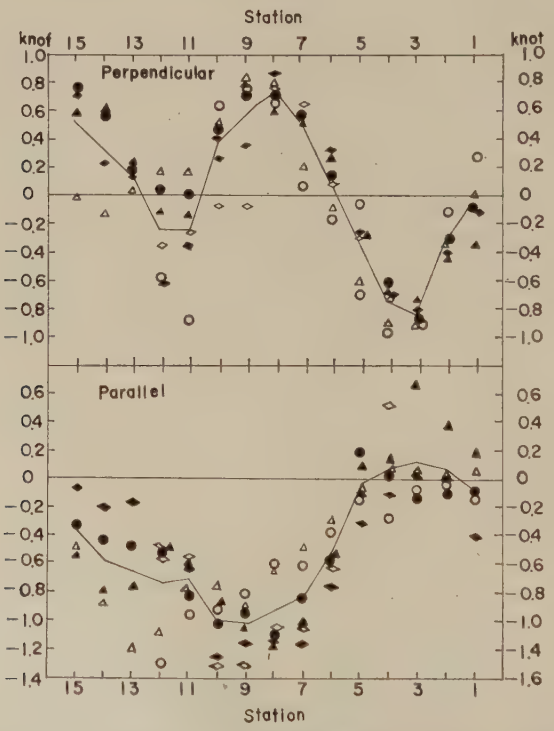

Fig. 12. Fluctuation of two components of surface current.
△: Section I ○: Section II ◇: Section III
▲: Section IV ●: Section V ◆: Section VI
Full lines are drawn by connecting mean values at each station.

combination of σ_1^2 and a^2 as shown above. Correlation coefficients of σ_1^2 and a^2 with σ^2 exhibit extent of their contribution to σ^2 (Table 3). Both σ_1^2 and a^2 are effective except at 100 m, 150 m and 200 m depths. a^2 plays an important role at 100 m and 150 m depths, while σ_1^2 does at 200 m depth. It is interesting that short-term fluctuation prevails at 200 m depth though it does not at 100 m and 150 m depths.

Fig. 12 shows the fluctuation of NE- and NW-components of surface current. Full lines are drawn by connecting mean values and present characteristic features in Fig. 6. Deviations from the mean value depend upon stations. Though the observations are made under stable conditions, deviations are large at some stations. This is partly caused by fluctuations of short period less than one day. The maximum value of standard deviation is about 0.3 knot (Fig. 13). Trend of surface current is obtained in the way which is used for temperature. The greatest magnitude reaches 0.15 knot/day and the distribution of trend is characteristic (Fig. 13). NW-component increases to the north of St. 11. This increase corresponds well to increase of temperature below the surface layer. Based on the variation of temperature and this current component, the following estimation is possible: large gradient of temperature is reduced by invasion of warm water and then southeastward speed decreases. The southeastward movement of the high speed zone is proved by increase

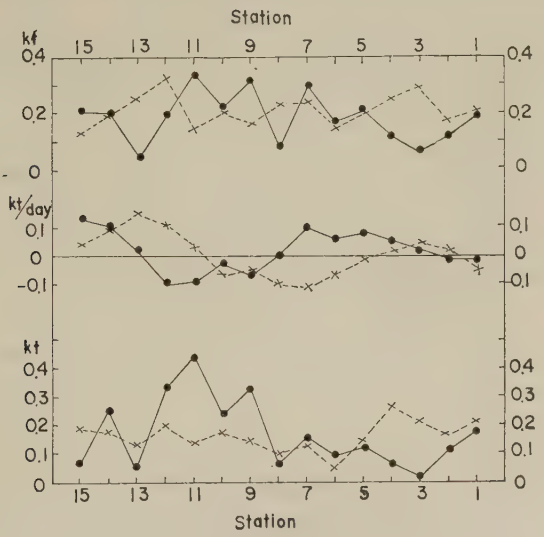

Fig. 13. Indexes indicating extent of fluctuation of surface current.
upper: σ middle: a lower: σ_1
●: NE-component ×: NW-component

of NE-component of current. Marked negative trend of temperature around St. 9 also suggests this movement. Magnitude of trend and σ_1 for NE-component are large where σ is large. This is the same situation as that obtained for temperature. For NW-component, on the other hand, the situation is not clear. σ_1 seems to be independent of σ and σ^2 is dependent on a^2 and combined effects of the trend with deviation from the linear variation, $\frac{a}{n}\sum_{i=1}^{n} t_i z_i$. Thus, for NE-component, fluctuations of long period and of short period are predominant where standard deviation is large, while for NW-component this characteristic feature is not found. Features described above are made clear by correlation coefficients (Table 3). It is interesting that short-term fluctuation prevails in NE-component but not in NW-component.

Correspondence of magnitude of trend and σ_1^2 between temperature and surface current is examined on the basis of Fig. 10 and Fig. 13. σ_1 is large for temperature and for NE-component of surface current to the north of St. 9, that is, short-term fluctuation of NE-component is predominant where short-term fluctuation of temperature above 50 m depth is predominant, and the correspondence between the two elements is good for short-term fluctuation in the upper layer. Correlation is examined between surface current and temperature (Table 4). At first, NE-component is taken. Correlation coefficients of σ_1^2 is great between NE-component and temperature at the surface, 10 m, 20 m, 30 m and 50 m depths. In other words, behaviours of short-term fluctuation of NE-component and temperature are same for the surface layer. There is no high correlation in σ^2 and a. Next, NW-component is taken.

Table 4. Correlation coefficients of σ^2, σ_1^2 and a between surface current and temperature.

NE-component

	0m	10m	20m	30m	50m	75m	100m	150m	200m
σ^2	0.526*	0.569*	0.484*	0.448*	0.364*	0.202*	0.401*	0.023*	−0.405*
σ_1^2	0.874	0.870	0.859	0.780	0.651	−0.058*	0.074*	−0.061*	−0.194*
a	0.250*	0.247*	0.189*	−0.003*	−0.100*	−0.122*	−0.174*	−0.146*	−0.290*

NW-component

	0m	10m	20m	30m	50m	75m	100m	150m	200m
σ^2	−0.192*	−0.191*	0.038*	0.074*	0.403*	0.831	0.556*	−0.402*	−0.140*
σ_1^2	−0.095*	−0.098*	−0.117*	−0.177*	−0.074*	−0.096*	−0.265*	0.128*	0.405*
a	0.272*	0.313*	0.454*	0.628*	0.800	0.853	0.800	0.480*	0.451*

Values with * are less than 1% point.

High correlation is found in a with temperature at 50 m, 75 m and 100 m depths, and not in σ_1^2. This suggests variation in the northern part of the section. Namely, warm water moved northeastward and temperature gradient in NE became small near this section and then southeastward speed decreased. Though difference in the correlation between NE- and NW-components may be attributed to chance, it is very interesting.

4. Observation at fixed stations

Direct current measurements and BT observations were tried on board the *Ryofu Maru*, who was anchored in the strong current. The purpose is to see the short-term fluctuation of current and water temperature. The first trial was made at St. T (39°23′N, 135°32′E) from 14 LST on 26 October to 19 LST on 28 October and the second at St. U (39°11′N, 135°42′E) from 20 LST on 29 October to 18 LST on 31 October (Fig. 1). In the first trial, however, anchoring the vessel failed and obtained data are not fit for the study.

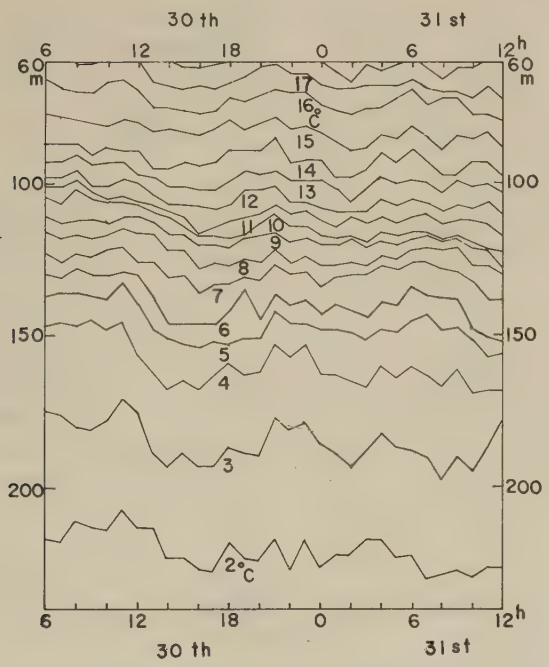

Fig. 14. Variation in depth of isotherm at St. U.

St. U in the second trial is located slightly north of the stream axis and about 1500 m deep. BT observations were made down to 250 m depth every hour and current measurements at 10 m, 30 m, 50 m, 100 m and 200 m depths every two hours. Since the vessel drifted before 06 LST on 30 and after 12 LST on 31, data between the two hours are used in the following discussions. Sampling interval is one or two hours and the duration of sampling is 31 hours, and then the number of samples is not sufficient. Thus, strict statistical method cannot be applied to the study.

Fluctuation of depth of isotherms is presented by BT observation (Fig. 14). Based on these samples, serial correlation coefficients are computed for the depth of 16°C–2°C isotherms. Here, 15 lags are taken though number of the longest lag is too great from the standpoint of statistics. The correlogram is shown in Fig. 15. For 16°C–12°C isotherms, a trough is around the 6th lag and a peak around the 10th lag. The feature is not so clear for 15°C and 12°C isotherms. For 11°C to 5°C isotherms, correlation coefficient decreases as lag number increases. For 4°C and 3°C isotherms, a trough is around the 8th lag and then coefficient increases with lag number. For 2°C isotherm, correlation coefficient decreases as lag number

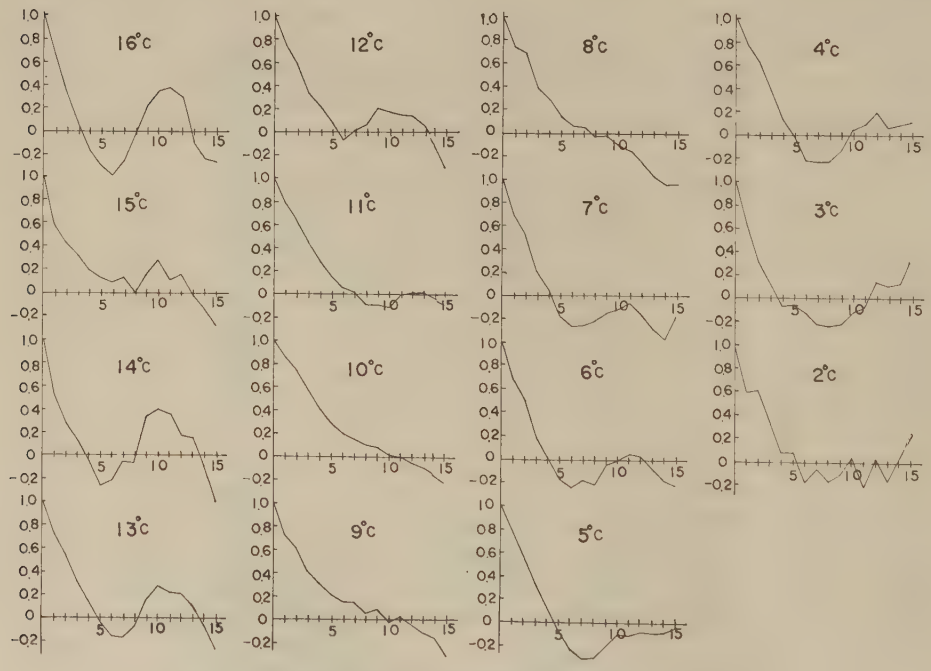

Fig. 15. Correlograms of depth of isotherm at St. U.

increases, and then, it oscillates. As mentioned above, there are not enough samples for strict statistical discussions. Correlogram, however, suggests that periods of about 10 hours and about 16 hours are predominant for 16°C–12°C isotherms and for 4°C and 3°C isotherms, respectively. The period of inertial oscillation is 19.01 hours at the latitude of 39°11′N. The results prove neither tidal oscillation nor inertial oscillation. It may be inferred at least that the period is longer for 4°C and 3°C isotherms (at 150–200 m depth) than for 16°C–12°C isotherms (at 70–110 m depth) and that periodicity is not found for other isotherms. This means that periodic vertical oscillation of isotherms is predominant in the upper part of thermocline and below it. The range of vertical displacement of isotherms is between 11 m for 14°C isotherm and 24 m for 4°C isotherm. For 2°C–6°C isotherms, the range is greater than 20 m, that is vertical displacement is marked in the lower part of thermocline and below it.

Neither tidal nor inertial period are clear in vertical displacement of isotherms on the correlogram shown in Fig. 15. The harmonic analysis, however, is tried because oscillations of tidal and inertial period are expected to exist in general cases. Mean depths and amplitudes are shown in Table 5. Semi-diurnal oscillation has

Table 5. Results of harmonic analysis of depth of isotherms at St. U. Origin of time is 05 LST on 30 October.

		Tidal				Inertial	
		Diurnal		Semi-diurnal			
	Mean	Amp.	Phase	Amp.	Phase	Amp.	Phase
16°C	73m	0.9m	216°	2.6m	284°	1.5m	206°
15	83	1.7	325	2.1	270	1.2	122
14	92	0.8	324	2.7	265	1.2	138
13	99	1.4	262	2.6	283	1.1	212
12	105	1.8	270	2.4	282	0.9	222
11	110	2.2	246	2.4	309	2.4	237
10	114	3.1	271	2.4	324	2.6	246
9	117	2.4	264	1.5	331	2.1	261
8	123	3.7	253	1.4	327	3.2	283
7	129	3.0	216	1.1	311	3.6	260
6	139	3.5	216	3.1	295	4.5	245
5	147	3.7	213	3.8	312	5.2	240
4	160	2.0	222	5.1	297	4.6	212
3	186	1.3	205	4.3	324	3.8	200
2	221	2.2	247	2.7	348	3.5	242

large amplitude for 16°C–11°C isotherms and inertial oscillation for 7°C–5°C and 2°C isotherms. Namely, tidal oscillation predomidates in the upper part of thermocline, while inertial oscillation does in the lower part of thermocline. This is consistent with the inference drawn on periodicity that the period is longer in the lower part than in the upper part of thermocline. For 3°C and 4°C isotherms, semi-diurnal oscillation has larger amplitude. But, the correlogram (Fig. 15) does not support that this oscillation is predominant for these isotherms.

Direct current measurements were made at 10 m, 30 m, 50 m, 100 m and 200 m depths every two hours and 13 or 14 samples are available. Direction of current was ESE at the four depths (10 m, 30 m, 50 m and 100 m) with a few exceptions. This means that mean speed is high enough to keep the direction of current unchanged. Mean speed decreases linearly from about 78 cm/sec at 10 m depth to about 4 cm/sec at 200 m depth. Amount of samples is not large and statistical discussion is impossible. Fluctuations of E-component and N-component of current velocity are shown in Fig. 16. Based on this figure, components surely fluctuate and most of them are subject to peiodic variation. It is not reasonable to make harmonic analysis for assumed periods as in the oscillation of isotherms. But, it is natural to assume tidal periods and inertial period. The results of analysis are given

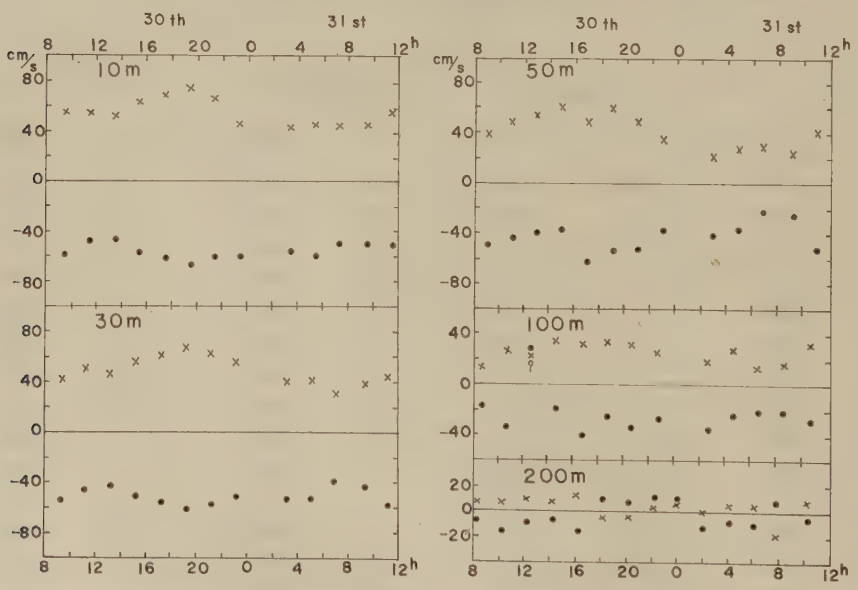

Fig. 16. Variation of current velocity at St. U.
●: N-component ×: E-component

Table 6. Results of harmonic analysis of current velocity for tidal oscillation at St. U. Origin of time is 05 LST on 30 October.

Depth	N-component					E-component				
	Mean	Diurnal		Semi-diurnal		Mean	Diurnal		Semi-diurnal	
		Amp.	Phase	Amp.	Phase		Amp.	Phase	Amp.	Phase
	cm/sec	cm/sec		cm/sec		cm/sec	cm/sec		cm/sec	
10m	−56	6.9	59°	3.0	204°	54	12.6	183°	5.6	49°
30	−50	6.4	54	1.8	206	50	13.6	201	2.0	115
50	−41	11.7	13	0.2	25	40	17.6	162	0.9	259
100	−24	10.7	92	6.3	221	25	7.1	185	1.4	335
200	− 3	7.4	249	7.9	96	2	3.3	150	6.5	242

Table 7. Results of harmonic analysis of current velocity for inertial oscillation at St. U. Origin of time is 05 LST on 30 October.

Depth	N-component		E-component		Ratio of Amp. N : E	Phase N. +90°	Diff. toward E
	Amp.	Phase	Amp.	Phase			
	cm/sec		cm/sec				
10m	5.9	129°	12.4	257°	0.48	219°	2.00h
30	5.7	120	12.5	284	0.46	210	3.86
50	9.5	97	13.6	239	0.70	187	2.75
100	8.5	139	6.7	253	1.27	229	1.27
200	10.1	307	1.5	107	6.73	37	3.68

in Tables 6 and 7. Amplitudes of diurnal tide are much greater than those of semi-diurnal tide except at 200 m depth, where amplitude of semi-diurnal tide is a little greater and amounts to about 10 cm/sec. The greatest amplitude of diurnal tide is about 20 cm/sec at 50 m depth. Direction of main axis of tidal ellipse is ESE-WNW at 10 m, 30 m, and 50 m depths and the fluctuation is predominant in the direction of mean current and in the opposite direction. At 100 m and 200 m depths, the direction is N–S. The characters for diurnal tide are obtained for inertial period, as well. Inertial motion on the earth is necessarily anticyclonic, and can be considered as a circular path in small-scale processes (VON ARX, 1962). Based on the results of harmonic analysis (Table 7), the motion is not close to inertial motion. Though the motion is anticyclonic, the path of particle is not circular but forms an ellipse of large eccentricity. The motion at 100 m depth is most close to inertial motion. Theoretically, ratio of amplitude of the two components is equal to one and the phase of N-component is larger by 90° than the phase of E-component.

Error in the results of analysis is caused by measurements themselves and by interpolation in data processing. But, the error will not be so great that characters of inertial motion are distorted. It is expected that oscillation of isotherms is connected with fluctuation of current. Close relation, however, is not found between them in the results of analysis.

5. Concluding remarks

The plan of observation was not finished for various reasons and small samples made statistical discussions impossible. Therefore, speculative inferences are drawn on fluctuations of the Tsushima Current and the warm water region. Though this situation is not desirable, it is expected that general features of their short-term fluctuation are inferred. In this study, estimation of error is not tried on the position of hydrographic stations and the depth of observed layer. But, these errors are supposed to be not so large that the inferences drawn here are overthrown. This study presents an example of short-term fluctuation and will serve as the one step of such a study on short-term fluctuation of the Tsushima Current, though it has a few weak points.

Acknowledgements

The author is indebted to all the officers, crew and observers on board five participating vessels. He also wishes to express his gratitude to Dr. J. MASUZAWA of the Japan Meteorological Agency and Dr. M. MIYAZAKI of the Metorological Research Institute for their advices and discussions through this work and to Miss K. OKADA of the Meteorological Research Institute for her assistance in data processing and preparing manuscript.

References

VON ARX, W.S. (1962); *An introduction to physical oceanography.* Addison-Wesley Publishing Co., Inc. pp. 422.

YI, SOK-U (1966): Seasonal and secular variations of the water volume transport across the Korea Strait. *Journ. Oceanogr. Soc. Korea,* 1(1–2), 7–13.

1969 年 10 月の能登半島北西沖における対馬海流の短期変動について

森　安　茂　雄

（気象研究所）

1969 年 10 月に能登半島北西沖で対馬海流の短期変動の観測を行なった．この観測では定線上の反復観測と碇置点における連続観測を実施した．天候そのほかの制約を受けて観測期間が短かく，厳密な統計的取扱いをすることはできなかったが，水温と流れについての変動の概略を示した．また，水温の変動と表面流の変動との間の関係について考察した．

The Oceanographical Magazine
Vol. 24, No. 1, pp. 25 to 38, December 1972

A preliminary report of the cruise of the R/V *Ryofu-Maru* in January-March 1971

Koichi NAGASAKA and Tsutomu SAWARA

Japan Meteorological Agency

(Received September 7, 1972)

Abstract: A hydrographic survey was carried out in the western North-Pacific in winter, 1971 on board the R/V *Ryofu-Maru*. The aims of the cruise were to make a long oceanographical section at 137°E meridian, which has been intensively studied in January by J.M.A. since 1967, and to observe the general features of the Kuroshio south of Japan.

The geostrophic flux across 137°E was computed and compared with those of the previous four surveys by J.M.A. It can be emphasized that the net flux of the North Equatorial Current was almost constant ($56.3 \pm 5.6 \times 10^6 m^3 \cdot s^{-1}$) throughout those winters though its width fluctuated greatly. The direct current measurements of the Equatorial Currents suggest that the boundaries and speed of the zonal currents were revealed as expected from geostrophic computation.

1. Introduction

An oceanographic cruise in the western North-Pacific was carried out in Jaunary-March 1971 by the R/V *Ryofu-Maru* of the Japan Meteorological Agency (J. M. A.). The cruise principally has two purposes. In the first half of the period a long meridional oceanographic section at 137°E from Japan to New Guinea was made across the major zonal currents. The section was surveyed four times by the R/V *Ryofu-Maru* since 1967 as a part of the C. S. K. (Cooperative Study of the Kuroshio and Adjacent Regions) project (MASUZAWA, 1967, 1968; AKAMATU and SAWARA, 1969; MASUZAWA *et al.*, 1970). In the last part of the period it was intended to observe the oceanic conditions south of Japan, especially the shape of the path of the Kuroshio. This report aimed to describe the outline of the survey and its results, chiefly the zonal currents across 137°E meridian.

2. The outline of the survey

The R/V *Ryofu-Maru* departed from Tokyo on January 13, 1971 and returned

on March 2. On her way she called at the ports of Ishigaki and Naha and the cruise logged 8,300 miles as given in Fig. 1. The observations on the section at 137°E was started on January 14 at 34°01′N just south of Cape Daiozaki and terminated at 1°00′S near the coast of New Guinea on January 28. The observations in

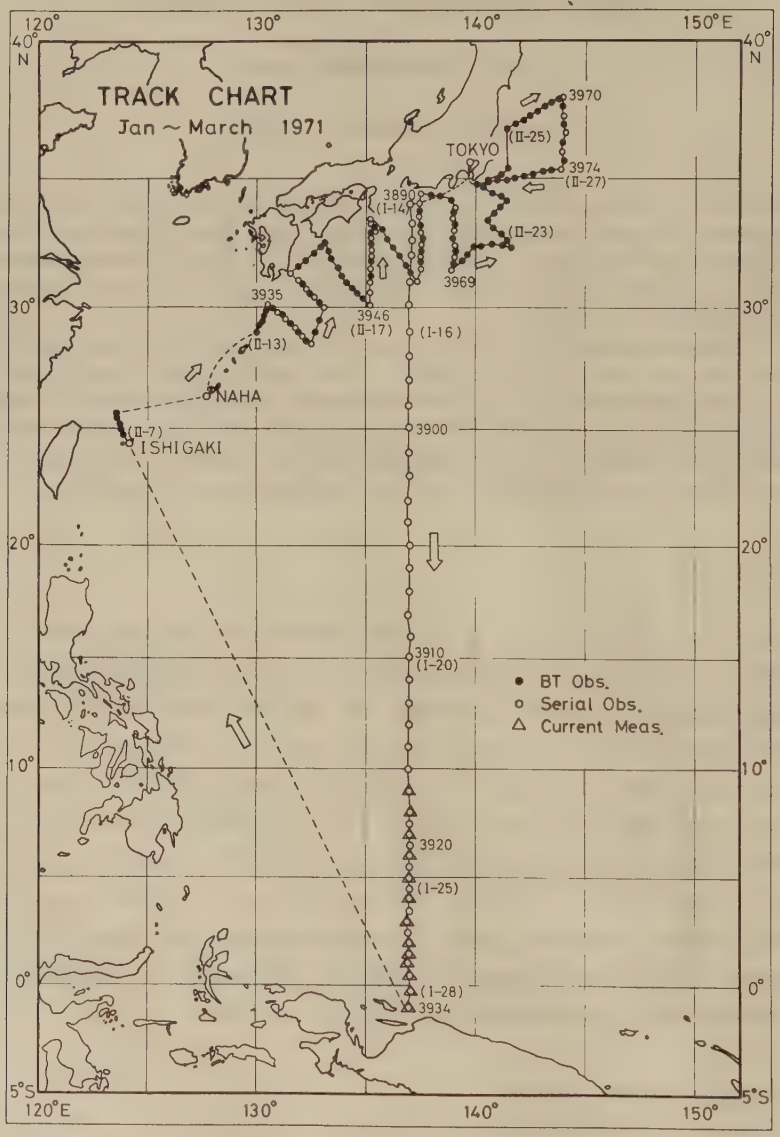

Fig. 1. Track chart of the cruise of the *Ryofu-Maru* in January to March 1971.

the previous four years by the *Ryofu-Maru* were also made in the same winter time.

In this section the standard hydrographic casts in the upper 1,200 m or deeper layer were done at 36 stations in every 60 miles as a rule. In addition to these stations 9 shallow hydrographic casts in the upper 500 m were settled one each at a middle point between two adjacent standard hydrographic casts in the Kuroshio region and south of 8°N to reveal the complicated structure of the sub-surface water. At 137°E section, 45 hydrographic casts were carried out in total. Sampling depths were chosen as follows;

North of 20°N ..... 0, 25, 50, 100, 125, 150, 175, 200, 300, 400, 500, 600, 700, 800, 900, 1,000, 1,200, (1,500) (2,000), ... m

8°N–20°N ..... 0, 10, 25, 50, 75, 100, 125, 150, 175, 200, 250, 300, 350, 400, 450, 500, 600, 700, 800, 900, 1,000, 1,200, (1,500), ... m

South of 8°N ..... 0, 10, 20, 30, 50, 75, 100, 125, 150, 175, 200, 225, 250, 275, 300, 350, 400, 450, 500, 600, 700, 800, 900, 1,000, 1,200, 1,400, 1,600, (2,000), (2,500), ... m

A bathythermograph was lowered at every station. The current in the upper 500 m was directly measured from drifting ship by two TS-II (Robert Type) current meters at 13 stations south of 9°N. The effect of the ship drift was corrected by the record of a current meter lowered at a depth of about 800 m.

Chemical elements such as salinity, oxygen, phosphate-P, silicate-Si, nitrate-N, nitrite-N and carbon dioxid in the surface water were determined at every station. Chlorophyll-a and phaeopigment in the upper 300 m were also measured on board by the fluorometric method. Standard sampling of zooplankton was made at each station (MASUZAWA, 1968).

On the last part of the cruise 131 GEK and 139 BT observations were carried out every 10 miles or so to follow the path of the Kuroshio. In 7 sections across the Kuroshio, 41 standard hydrographic casts were also made.

3. Results

(1) *The section at 137°E*

The section at 137°E can be divided into the following six current zones: the Kuroshio, its countercurrent, the subtropical zone, the North Equatorial Current, the Equatorial Countercurrent and the South Equatorial Current, away from the coast of Japan in the order named. In addition to these currents the presence of the

Equatorial Undercurrent is reported by many authors (YOSHIDA *et al.*, 1959; TSUCHIYA, 1961 and 1968, etc.).

The boundaries of each zonal current are clearly revealed by the pattern of the geopotential anomaly on isobaric surfaces. They are summarized in Table 1. The table contains not only the characteristic properties of each zonal current in 1971

Table 1. Characteristic properties of zonal currents through the section at 137°E

Current	Item ＼ Year	1967
Kuroshio	Range	Ry. 3031–Ry. 3035
		33°28′N–31°18′N
	Width (mile)	130
	$\Delta\phi$ (dyn·cm)	−117
	Flux ($\times 10^6 m^3 \cdot s^{-1}$)	−75.5
Kuroshio Countercurrent	Range	Ry. 3035–Ry. 3038
		31°18′N–28°54′N
	Width (mile)	144
	$\Delta\phi$ (dyn·cm)	+47
	Flux ($\times 10^6 m^3 \cdot s^{-1}$)	+45.0
Subtropics	Range	Ry. 3038–Ry. 3045
		28°54′N–21°58′N
	Width (mile)	416
	$\Delta\phi$ (dyn·cm)	−16
	Flux ($\times 10^6 m^3 \cdot s^{-1}$)	+0.2
North Equatorial current	Range	Ry. 3045–Ry. 3060
		21°58′N–06°58′N
	Width (mile)	900
	$\Delta\phi$ (dyn·cm)	+55
	Flux ($\times 10^6 m^3 \cdot s^{-1}$)	+57.9
Equatrorial Countercurrent	Range	Ry. 3060–Ry. 3065
		06°58′N–02°04′N
	Width (mile)	294
	$\Delta\phi$ (dyn·cm)	−28
	Flux ($\times 10^6 m^3 \cdot s^{-1}$)	−65.1
South Equatorial current	Range	Ry. 3065–Ry. 3070
		02°04′N–00°43′S
	Width (mile)	167
	$\Delta\phi$ (dyn·cm)	?
	Flux ($\times 10^6 m^3 \cdot s^{-1}$)	?

but also those of the previous four serveys by the R/V *Ryofu-Maru*. The geostrophic flux through an area with 60 miles in width and 100 m in thickness and the net flux for each 60 miles in the upper 1,000 m layer are respectively given in Figs. 3 and 4. The depth of 1,000 m was commonly chosen for the reference level in the present geostrophic computation.

in January from 1967 to 1971. The flux in positive sign means westward flow.

1968	1969	1970	1971
?	Ry. 3394–Ry. 3399	?	Ry. 3890–Ry. 3894
?	34°00′N–31°22′N	?	34°01′N–31°00′N
?	158	?	181
?	?	?	−89
?	?	?	−61.3
? –Ry. 3186	Ry. 3399–Ry. 3403	? –Ry. 3624	Ry. 3894–Ry. 3896
? –27°59′N	31°22′N–28°00′N	? –29°00′N	31°00′N–29°01′N
>120	202	?	119
?	+32	?	+28
?	+24.1	?	+20.7
Ry. 3186–Ry. 3192	Ry. 3403–Ry. 3410	Ry. 3624–Ry. 3634	Ry. 3896–Ry. 3906
27°59′N–22°00′N	28°00′N–20°58′N	29°00′N–19°00′N	29°01′N–19°01′N
359	422	600	600
−15	−22	−7	−25
+2.7	+1.2	+5.9	+4.8
Ry. 3192–Ry. 3206	Ry. 3410–Ry. 3423	Ry. 3634–Ry. 3647	Ry. 3906–Ry. 3917
22°00′N–07°58′N	20°58′N–07°59′N	19°00′N–07°00′N	19°01′N–08°02′N
842	779	720	659
+52	+63	+35	+54
+59.6	+60.9	+46.8	+56.4
Ry. 3206–Ry. 3220	Ry. 3423–Ry. 3437	Ry. 3641–Ry. 3655	Ry. 3917–Ry. 3925
07°58′N–00°58′N	07°59′N–01°00′N	07°00′N–03°00′N	08°02′N–04°02′N
420	419	240	240
−28	?	−30	−27
−47.3	?	−44.6	−29.8
Ry. 3220–Ry. 3225	Ry. 3437–Ry. 3441	Ry. 3655–Ry. 3662	Ry. 3925–Ry. 3934
00°58′N–01°58′S	01°00′N–01°00′S	03°00′N–01°00′S	04°02′N–01°00′S
125	120	240	302
?	?	?	?
?	?	?	?

a) The Kuroshio and its countercurrent

An area of 180-mile interval between Ry-3890 (34°01′N) and Ry-3894 (31°00′N) is occupied by the Kuroshio and the difference in geopotential between both ends is 89 dyn. cm. The total flux is $61.3 \times 10^6 m^3 \cdot s^{-1}$. These are reasonable when they are compared with the values commonly estimated (MASUZAWA, 1965). The interval between the stations seems to be too large to estimate the exact width of the Kuroshio in this observation and our estimate of 180 miles for the width could be too

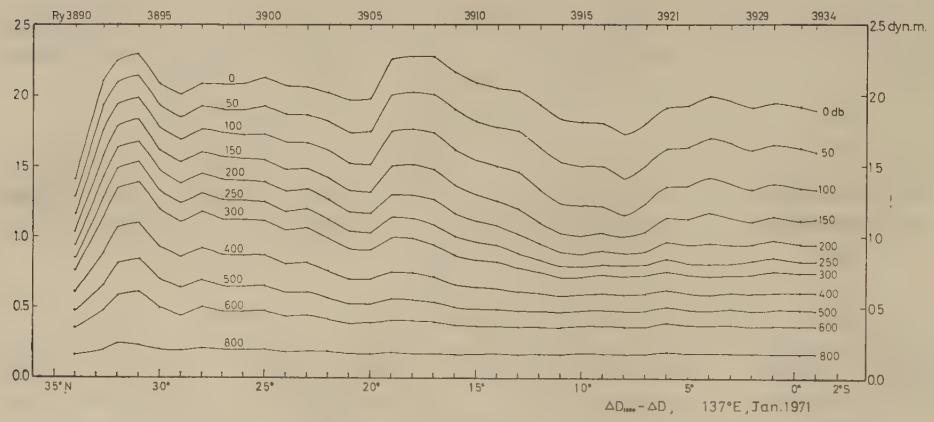

(a)

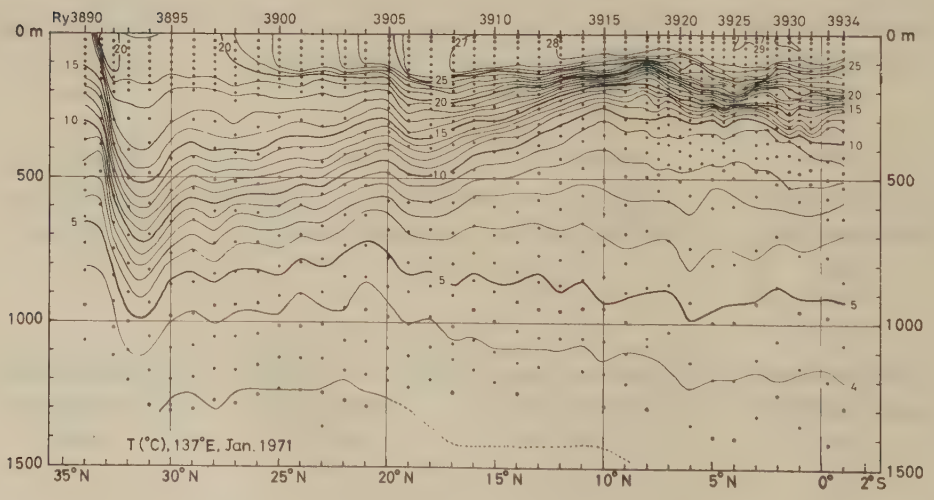

(b)

large. South of the Kuroshio there exists a clear westward current, which corresponds to the Kuroshio Countercurrent. The westward flux and the difference in geopotential between both boundaries are respectively $20.7 \times 10^6 m^3 \cdot s^{-1}$ and 28 dyn. cm. They seem to be the smallest among the five cruises by the R/V *Ryofu-Maru*.

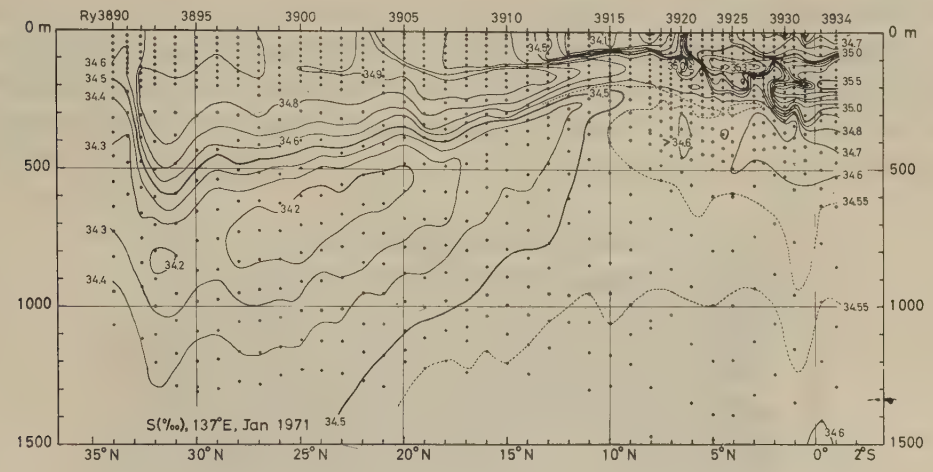

(c)

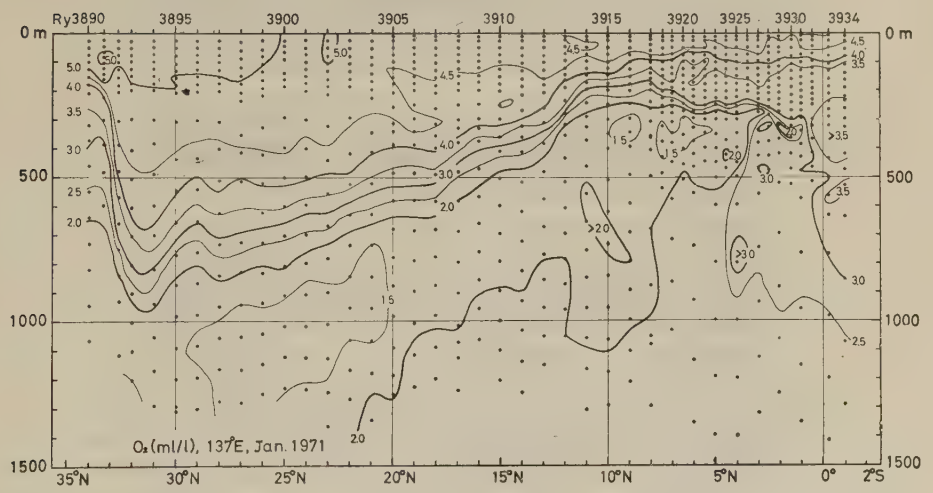

(d)

Fig. 2. Vertical sections at 137°E by the *Ryofu-Maru* in January 1971; (a) geopotential anomaly relative to 1,000 db, (b) temperature, (c) salinity, and (d) oxygen content. Vertical exaggeration is 1480.

However, it is unfortunate that in 1968 and 1970 the section did not cover the whole width of the Kuroshio Countercurrent.

The sea surface temperature in the Kuroshio region in 1971 is the highest of the recent five winters and normal in its counter current. The salinity of the surface water is the lowest in both regions.

b) Subtropics

Between Ry-3896 (29°01′N) and Ry-3906 (19°01′N) there is a zone where current is variable in direction. The net westward flux of $4.8 \times 10^6 m^3 \cdot s^{-1}$ is almost the same as the flux in 1970, when most part of this region was occupied by uniform westward current. But the fluxes in 1970 and 1971 are larger than those in 1967, 1968 and

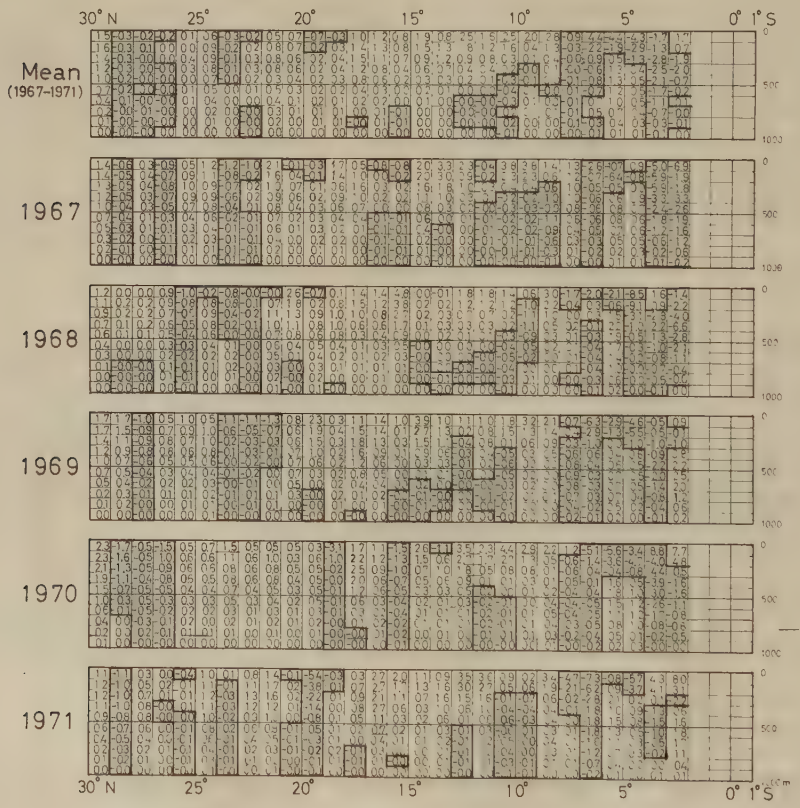

Fig. 3. Vertical distribution of the geostrophic flux at 137°E section referred to 1,000 db surface in January from 1967 to 1971 by the *Ryofu-Maru*. A numeral means a geostrophic flux through an area of 60 miles×100 m and the positive sign indicates westward flux. Unit is in $10^6 m^3 \cdot s^{-1}$.

1969 in which years only weak and narrow westward or eastward currents appeared. It is noteworthy that a narrow but very strong current zone in eastward direction is observed at the southern edge of this area. The current speed estimated by geopotential exceeds 50 cm·s^{-1} in the upper 50 m layer in 1971. Similar swift current was also observed in 1970, but its flux in 1970, $3.5 \times 10^6 m^3 \cdot s^{-1}$, was less than 25% of the flux in 1971. As commonly observed in the previous four winters a fairly uniform and remarkable westward current appeared between 25°N and 21°N in 1971, too. The core of this westerly stream seems to be between 22°N and 21°N

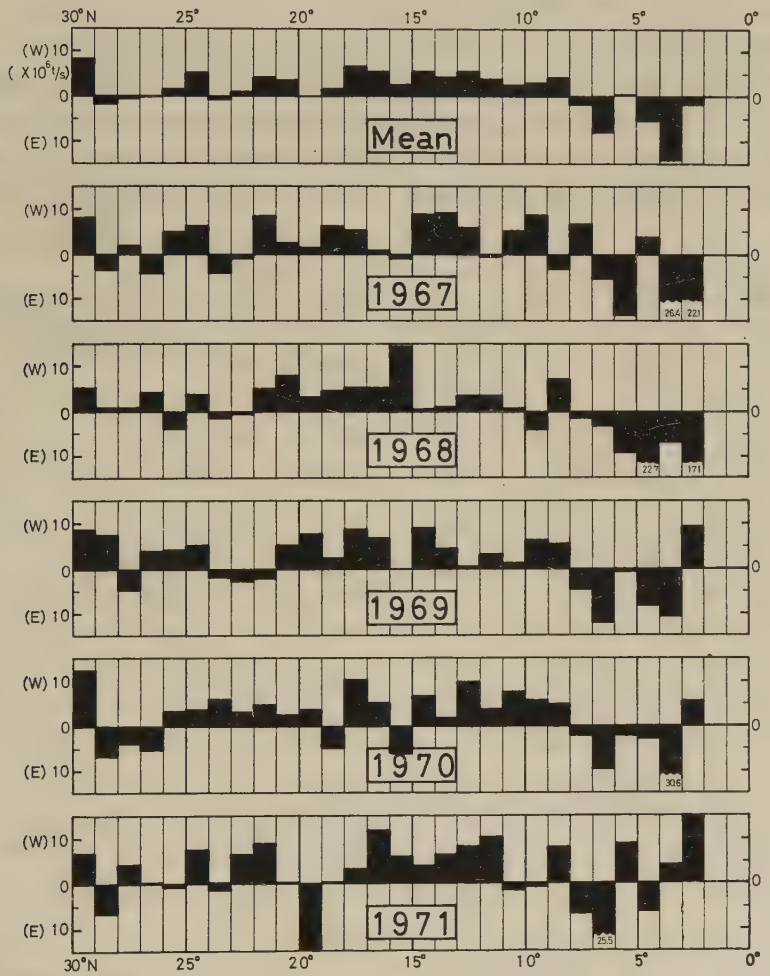

Fig. 4. The net flux at 137°E section in the upper 1,000 m for each 60 miles.

around 125 m in depth with the speed of 16 $cm \cdot s^{-1}$.

Both temperature and salinity at the sea surface in the Subtropical region are rather low in 1971 among the five winters.

c) The North Equatorial Current

To the south of the Subtropical zone a gentle and uniform slope of the isobaric surface is revealed over 659 miles, that is, about a third of the whole section. The difference in geopotential of the sea surface between the boundaries is 54 dyn. cm and the total flux is $56.4 \times 10^6 m^3 \cdot s^{-1}$. The characteristic indexes of the North Equatorial Current are summarized in Table 2, in which the indexes in summer season are also contained for the reference.

It should be emphasized that the net flux of the North Equatorial Current is almost constant with the mean value of $56.3 \times 10^6 m^3 \cdot s^{-1}$ through the five survey by the *Ryofu-Maru* in each January though its width fluctuates greatly. For instance, the ratio of the width in 1967 to it in 1971 exceeds 1.35, on the other hand the ratio of the net flux is 1.03. According to the limited examples given in Table 2 it

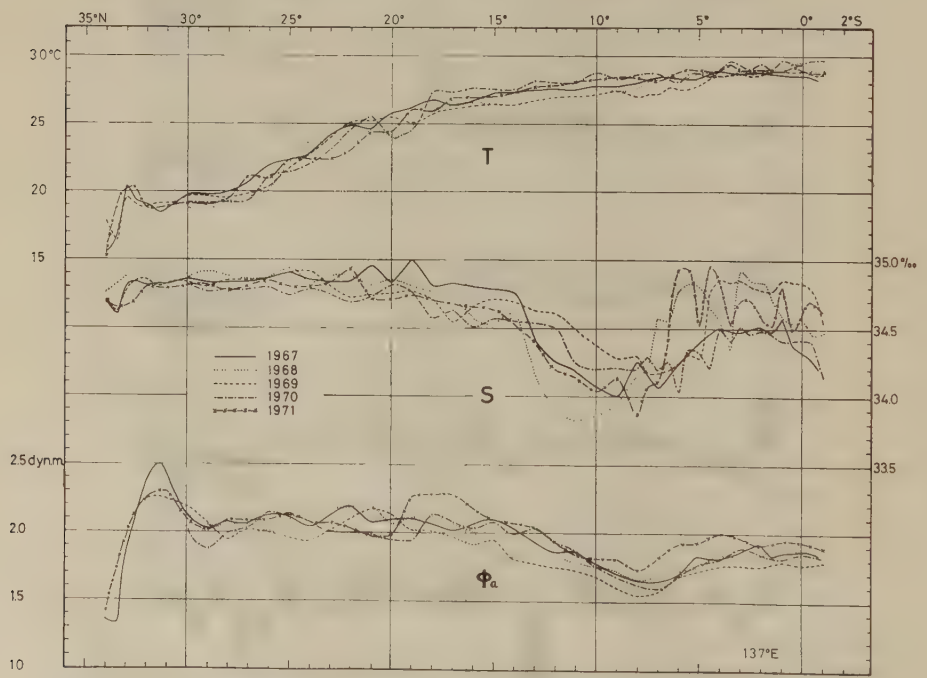

Fig. 5. Surface temperature, salinity and geopotential anomaly in 137°E meridian from 1967 to 1971.

Table 2. Characteristic indexes of the North Equatorial Current in the western North Pacific in winter (by the *Ryofu-Maru*) and in summer. The data in summer is from MASUZAWA (1970).

Date	Position	$\Delta\phi$ (dyn·cm)	North of 15°N		South of 15°N		Total		A/B (%)	C/D (%)
			Range (A)	Flux (C)	Range (mile)	Flux ($\times 10^6 m^3 \cdot s^{-1}$)	Range (B)	Flux (D)		
Jan. 1967	22–07N	55	424	21.4	476	36.5	900	57.9	47	37
Jan. 1968	22–08N	52	420	46.0	422	13.6	842	59.6	50	77
Jan. 1969	21–08N	63	358	31.4	421	29.5	779	60.9	46	52
Jan. 1970	19–07N	35	242	9.5	478	37.3	720	46.8	34	20
Jan. 1971	19–08N	54	239	22.3	420	34.1	659	56.4	36	34
Average		52	337	26.1	447	30.2	792	56.3	43	46
July 1939*	20–07N	65	300	41.4	480	21.4	780	62.8	38	66
July 1939**	20–08N	41	300	22.2	420	46.7	720	68.9	42	33
July 1956***	20–07N	56	300	21.7	480	45.6	780	67.3	38	32
Average		54	300	38.4	460	37.9	760	66.3	39	43

* Takunan-Maru VIII, ** Takunan-Maru X, *** Keiten-Maru

seems that the net flux in winter season is slightly smaller than in summer. But the difference of the total flux between winter and summer is still unknown. The routine observation in this section is expected to be done not only in winter but also in the other seasons.

As previously reported by MASUZAWA (1968), the region of the North Equatorial Current can be divided into the two parts with the boundary at 15°N from standpoints of the slope of isobaric surface below 500 m. This boundary does not seem to shift through the five Januaries. As shown in Table 2 the ratio of the ranges and the fluxes between the northern and southern parts are irregular in every survey. The relation among the ratios of these indexes and other parameters is one of the important problem in future.

The surface water in the North Equatorial Current zone is characterized by low salinity and high temperature in 1971. Especially in the southern part of the current the salinity in the sea surface is as remarkably low as in 1968

The saline water exceeded 35‰ in the subsurface depth did not appear in 1971 in this region. It was common that such saline water was observed at about 200 m depth, for example it was located between 20°N and 10°N in 1967, 21°N and 12°N in 1968, 21°N and 10°N in 1969 and around 12°N in 1970 respectively.

d) Equatorial Currents

The slope of the isobaric surface down to the north between 8°02′N and 4°02′N

corresponds to the Equatorial Countercurrent. The maximum current speed estimated by the geopotential difference exceeds 60 $cm \cdot s^{-1}$ between 6°N and 7°N in the upper 100 m layer. In the mid-depth layer around 5°N the westward current appears as observed in the previous four winters. The total flux of the Equatorial Countercurrent is $29.8 \times 10^6 m^3 \cdot s^{-1}$ in 1971. This is rather small compared with that in the previous winters.

In the present report the hydrostatic computation was hesitated to extend to the south of 2°N. However, to the south of 9°N the direct current measurements were carried out by the method described before. The results of the direct current measurements are fairly consistent with the geostrophic current.

In the south of the Equatorial Countercurrent the westerly current is revealed from the direct current observations. The southern part of this westward current is covered with a shallow and weak eastward current. This easterly current was usually observed near the coast of New Guinea in the northern winter. In some winter such as 1969 this shallow easterly current covered the whole region south of the Equatorial Countercurrent. In the mid-depth around 200 or 300 m a remarkable eastward stream was observed, which has two cores of the current speed at 1°30′N around 200 m and 1°00′N around 300 m. This eastward current seems to be connected to the Equatorial Countercurrent as already reported by many authors (YOSHIDA *et al.*, 1959; etc.) This eastward current seems to be an origin of the Equa-

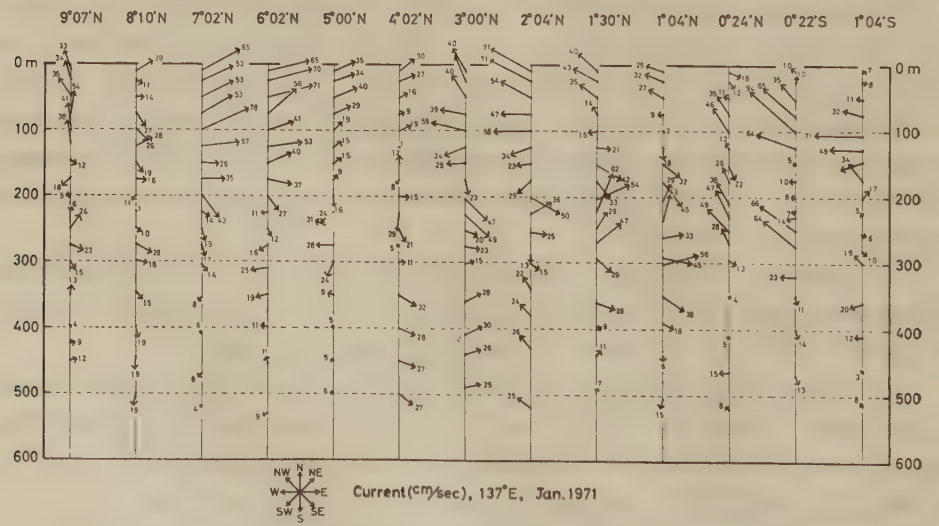

Fig. 6. Vertical distribution of current velocity measured relative to a depth of 800 m in the equatorial region.

torial Undercurrent.

In 1971 the surface temperature is rather high in the Equatorial Countercurrent, on the other hand it is low in the South Equatorial Current compared with those of the previous four winters. The saline water exceeding $35^0/_{00}$ in the subsurface depth around the equator occupied the region south of 5°N as commonly observed in the previous years. The oxygen content in the surface layer south of 5°N has never exceeded 4.5 cc/l in the four winters, but it exceeds 4.5 cc/l through out the whole section in 1971.

(2) The Kuroshio south of Japan

The Kuroshio approaches to Cape Shionomisaki through the Tokara Strait from East China Sea along the coast of Kyushu and Shikoku Islands. The path is at 30 miles off Cape Toimisaki, at 20 miles off Cape Ashizurimisaki and also at 20 miles off Cape Murotomisaki. South of Cape Shionomisaki the axis is located at only 10 miles of the coast and the current speed is 2.5 kt in the center of the axis. Then the path makes a detour around a large cold water mass in the Enshunada, at the center of which the temperature at 200 m depth is less than 11°C, and reaches the Boso Peninsula after meandering. It runs off to the ENE direction. To the north of this stream a warm water mass is observed, whose center is at 38°N and 143°E approximately.

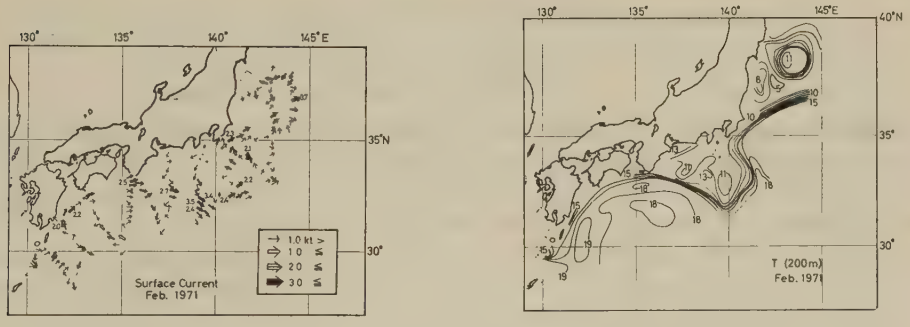

(a) (b)

Fig. 7. (a) Surface current by GEK, and (b) temperature at 200 m depth by BT south of Japan in February 1971.

Acknowledgements

The authors are grateful to members of the scientific party, officers and crew

aboard the *Ryofu-Maru* for their cooperation. They are also indebted to Dr. J. MASUZAWA in Marine Division, JMA for his constant encouragement.

References

AKAMATSU, H. and T. SAWARA (1969): The preliminary report of the third cruise for CSK, January to March 1969. *Oceanogr. Mag.*, **21**, 67–81.

MASUZAWA. J. (1965): Water characteristics of the Kuroshio. *Oceanogr. Mag.*, **17**, 37–48.

MASUZAWA, J. (1967): An oceanographic section from Japan to New Guinea at 137°E in January 1967. *Oceanogr. Mag.*, **19**, 95–118.

MASUZAWA, J. (1968): Second cruise for CSK, *Ryofu Maru*. *Oceanogr. Mag.*, **20**, 173–185.

MASUZAWA, J., T. AKIYAMA, Y. KAWARADA and T. SAWARA (1970): Preliminary report of the *Ryofu Maru* Cruise Ry-7001 in January-March 1970. *Oceanogr. Mag.*, **22**, 1–25.

MASUZAWA, J. (1970): Geostrophic flux of the North Equatorial Current south of Japan. *Jour. Oceanogr. Soc. Japan*, **26**, 61–64, (in Japanese).

TSUCHIYA, M. (1961): An oceanographical description of the equatorial current system of the western Pacific. *Oceanogr. Mag.*, **13**, 1–30.

TSUCHIYA, M. (1968): Upper water of the Intertropical Pacific Ocean. *Johns Hopkins Oceanographic Studies*, **4**, 50 pp.

YOSHIDA, S., H. NITANI and N. SUZUKI (1959): Report of multiple ship survey in the equatorial region (IGY), Jan.-Feb., 1958, *Bull. Hydrographic Office*, **59**, 1–30, (in Japanese).

1971 年 1～3 月凌風丸海洋観測報告

長 坂 昂 一・佐 原　　勉

（気象庁海洋気象部）

1971 年 1 月から 3 月にかけて，凌風丸により東経 137 度線上及び日本南方の海洋観測を実施した．このうち東経 137 度線上の観測は，1967 年から毎冬定期的に行なっているものであり，今回も前とほぼ同様な観測を実施した．即ち，日本沿岸から，ニューギニア沖までの約2000マイルの間に 45 点の各層観測，さらに赤道付近では，TS-II 型流速計による 2 機測流を行なった．

東経 137 度線上には，各種の帯状東西流があるが，これらの流量・流速等を 1967～71 年の 5 年間について算出した結果（図 4 及び 5），特に注目すべきことは，北赤道海流の流域巾の大きな変動にもかかわらず，その総流量は上記 5 年間の冬を通じてほぼ一定であるということである．

北緯 9 度以南で実施した直接測流と，北緯 3 度以北で求めた地衡流計算の結果を比較たところ，両者はかなり良く一致した．

後半の観測では，約 10 マイルごとに BT・GEK 観測を実施し黒潮流軸の追跡を行なった．

The Oceanographical Magazine
Vol. 24, No. 1, pp. 39 to 55, December 1972

Edge waves on the linearly sloping coast

——II. Forced waves and β-effect——

Hayato IIDA

Japan Meteorological Agency

(Received September 9, 1972)

Abstract: In this paper atmospheric disturbances propagating periodically along the coast are treated. In an extent of wave length and period of the disturbances, the response of the system is almost static and barotropic for pressure, while it is in phase and baroclinic for on-shore components of wind stress and out of phase, about $+90°$, and also baroclinic for long-shore components. Quantitative difference of the responses can not be found for the on- and long-shore components of wind stress.

The β-effect on the free modes of the system is considered in the range of wave numbers where it can be treated as a correction for the case $\beta=0$. The corrections due to the variability of the profiles off the coast are obtained in the same manner.

1. Introduction

In the previous paper (IIDA, 1970), the following facts are discussed:

(1) The differential equation for a rotating two-layered ocean can be separated into a system of two 2nd order ones which is feasible for mathematical treatment only when the change in depth is linear and the thicknesses of the layers are linear, too. In this case, the difference of velocities in the upper and lower layers can be expressed as

$$V_1 - V_2 = \frac{\Delta\rho}{\rho_2} g \frac{dh_1}{dx}, \tag{1-1}$$

where ρ_j, V_j and $h_j = s_j x$ are the density, y-component of the velocity in the undisturbed state and thickness of the upper layer (for $j=1$) and of the lower layer (for $j=2$), respectively.

(2) The system of the 2nd order differential equation to be solved is

$$\left(\frac{d}{dx} x \frac{d}{dx} - k^2 x\right)\zeta_j + \sum_{i=1}^{2} A_{ij}\zeta_i = 0, \quad j = 1, 2, \tag{1-2}$$

Table 1. Approximate formulae for

		$l=1$	$l=2$
$1 \gg \frac{g(s_1+s_2)}{f^2}k'$	$n=0$	$f+V_tk'+\frac{g(s_1+s_2)}{f}k'$	$V_tk'-\frac{g(s_1+s_2)}{f}k'$
	$n>0$	$f+V_tk'+(n+1)\frac{g(s_1+s_2)}{f}k'$	$-f+V_tk'-n\frac{g(s_1+s_2)}{f}k'$
$\frac{\rho_2}{\Delta\rho} \gg \frac{g(s_1+s_2)}{f^2}k'>1$	$n=0$	$\frac{f}{2}+V_tk'+\sqrt{\frac{f^2}{4}+g(_1s+s_2)k'}$	$\frac{f}{2}+V_tk'-\sqrt{\frac{f^2}{4}+g(s_1+s_2)k'}$
	$n>0$	$V_tk'+\sqrt{(2n+1)g(s_1+s_2)k'}$	$V_tk'-\sqrt{(2n+1)g(s_1+s_2)k'}$
$\frac{g(s_1+s_2)}{f^2}k' \sim \frac{\rho_2}{\Delta\rho}$	$n=0$	$\frac{f}{2}+V_tk'+\sqrt{g(s_1+s_2)k'}$	$\frac{f}{2}+V_tk'-\sqrt{g(s_1+s_2)k'}$
	$n>0$	$V_tk'+\sqrt{g(2n+1)(s_1+s_2)k'}$	$V_tk'-\sqrt{g(2n+1)(s_1+s_2)k'}$

* indicates that the root can not be expressed in the approximate form.

where A_{1j}'s are function of wave number k' and frequency σ, and ζ_j are the perturbation height of the surface (for $j=1$) and of the interface (for $j=2$), respectively. The boundary conditions ζ_j are finite both as $x\to 0$ and ∞.

(3) Then, the solutions of the above equation become confluent hypergeometric polyhomials $L_n(2k'x)e^{-k'x}$, where L_n is the n-th order Laguerre polynomial and n is a positive integer or 0.

(4) A 6th order algebraic equation concerning with frequency and wave number is obtained as the frequency equation of the system for $n>0$, where it reduces to a 4th order one for $n=0$. Solving the equation, the following expression (Table 1) are obtained for frequency σ;
where $V_t=(h_1V_1+h_2V_2)/(h_1+h_2)$, $V_c=(h_2V_1+h_1V_2)/(h_1+h_2)$.

(5) The numerical analysis of the frequency equation reveals that no instability occurs in this system.

(6) The characters of the above roots of the frequency equation are shown in table 2.

(7) For small wave numbers, the barotropic waves can be well approximated with the edge waves in a system of gravity g and homogeneous water of thickness

the roots of the frequency equation.

$l=3$	$l=4$	$l=5$	$l=6$
	$f+V_ck'+\frac{\Delta\rho}{\rho_2}g\frac{s_1s_2}{s_1+s_2}\frac{k'}{f}$	$V_ck'-\frac{\Delta\rho}{\rho_2}g\frac{s_1s_2}{s_1+s_2}\frac{k'}{f}$	
$V_tk'-\frac{g(s_1+s_2)}{f}k'$	$f+V_ck'+n\frac{\Delta\rho}{\rho_2}g\frac{s_1s_2}{s_1+s_2}\frac{k'}{f}$	$-f+V_ck'-n\frac{\Delta\rho}{\rho_2}g\frac{s_1s_2}{s_1+s_2}\frac{k'}{f}$	$V_ck'-\frac{\Delta\rho}{\rho_2}g\frac{s_1s_2}{s_1+s_2}\frac{k'}{f}$
	$f+V_ck'+\frac{\Delta\rho}{\rho_2}g\frac{s_1s_2}{s_1+s_2}\frac{k'}{f}$	$V_ck'-\frac{\Delta\rho}{\rho_2}g\frac{s_1s_2}{s_1+s_2}\frac{k'}{f}$	
$V_tk'-\frac{f}{2n+1}$	$f+V_ck'+n\frac{\Delta\rho}{\rho_2}g\frac{s_1s_2}{s_1+s_2}\frac{k'}{f}$	$-f+V_ck'-n\frac{\Delta\rho}{\rho_2}g\frac{s_1s_2}{s_1+s_2}\frac{k'}{f}$	$V_ck'-\frac{\Delta\rho}{\rho_2}g\frac{s_1s_2}{s_1+s_2}\frac{k'}{f}$
	$\frac{f}{2}+V_ck'$ $+\sqrt{\frac{f^2}{4}+\frac{\Delta\rho}{\rho_2}g\frac{s_1s_2}{s_1+s_2}k'}$	$\frac{f}{2}+V_ck'$ $-\sqrt{\frac{f^2}{4}+\frac{\Delta\rho}{\rho_2}g\frac{s_1s_2}{s_1+s_2}k'}$	
$V_tk'-\frac{f}{2n+1}$	$V_ck'+\sqrt{(2n+1)\frac{\Delta\rho}{\rho_2}g\frac{s_1s_2}{s_1+s_2}k'}$	$V_ck'-\sqrt{(2n+1)\frac{\Delta\rho}{\rho}g\frac{s_1s_2}{s_1+s_2}k'}$	*

Table 2. Character of the free modes.

species		$l=1$	$l=2$	$l=3$	$l=4$	$l=5$	$l=6$
$\frac{\rho_2}{\Delta\rho}\gg\frac{g(s_1+s_2)}{f^2}k'>1$	$n=0$	barotropic inertio-gravitational			baroclinic inertial	baroclinic quasi-geostrophic	
	$n>0$	barotropic inertio-gravitational			baroclinic inertial		quasi-geostrophic

(h_1+h_2), which are advected with velocity $(h_1V_1+h_2V_2)/(h_1+h_2)$. The baroclinic waves can be approximated with the waves in a system of gravity $(\Delta\rho/\rho_2)g$ and homogeneous water of thickness $h_1h_2/(h_1+h_2)$, which are advected with velocity $(h_2V_1+h_1V_2)/(h_1+h_2)$.

(8) In a physically interesting range of wave numbers, stationary waves are possible because of fundamental currents, that is, waves for $l=3$ and $l=6$ which propagate westwards at a comparatively slow speeds, become stationary.

Forced edge waves were studied by Reid (1958), Kajiura (1958), and so on, in more or less general ways. In this paper the forced waves are investigated in section 2. Response of the system to periodically propagating atmospheric disturbances

are discussed, which is very important for the problem of tidal data analysis and prediction of unusual tides, etc. Transient response of the system to the disturbances applied suddenly is more interesting, but it is very difficult to solve and resigned in this paper.

The long waves in the marginal sea of a β-plane ocean were studied by Yoshida (1960). Here the cases where the Colioris parameter and the inclinations of the surface and interface are variable with the distance from the coast, are treated in section 3. As it is difficult to solve these problems directly, too, the approximation in (7) mentioned above are used.

2. Forced Waves

Considering the sea south of Japan, atmospheric disturbances travel along the coast mostly from west to east, which are, of course, related to planetary waves of the atmosphere. These phenomena can be incorporated into this model as periodically travelling external disturbances. In this section the response of the system to such forces is investigated. In order to cosider the problem, free waves of the system are not necessarily important if there is some dissipating mechanism, however small it is, because, even though the external forces act suddenly, the characteristics of the motion in the system becomes the same as that of the external forces shortly after the time characteristic to the system. Here, for the sake of simplicity, the following external forces will be added to the system.

$$P_0,\ X \text{ and } Y \propto \exp(-k'x + ik'y - i\sigma t)$$

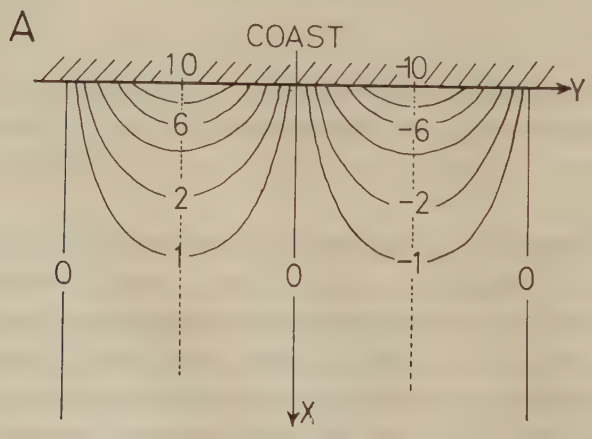

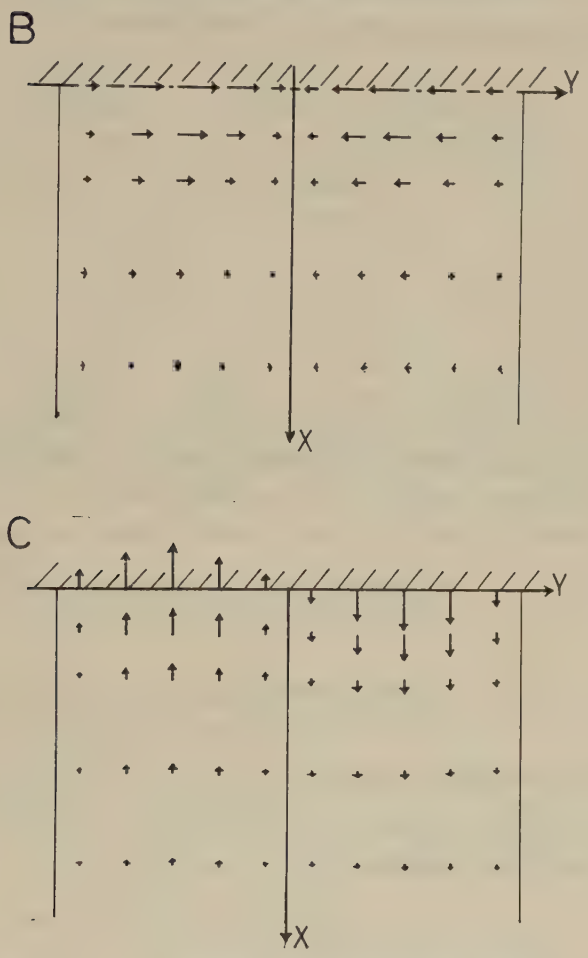

Fig. 1. Pattern of disturbance corresponding to the relation used in 2, A: pressure, B: X-component of wind stress, and C: Y-component.

which are shown in Figs. 1-a~b, where P_0, X and Y are the atmospheric pressure at the sea surface and x- and y-component of wind stress, respectively, and k' and σ are the wave number and frequency of the disturbance. The external forces expressed as the above formula can simulate the travelling disturbances along the coasts of Japan very well. The discussion of their effects to the system will be done separately.

(I) *Effect of pressure*

At first, only considering pressure as a disturbance propagating along the coast,

equation (2–22) in the previous paper (IIDA, 1970) becomes

$$-\left(1+\frac{1}{\omega_1}+\frac{1-\omega_1{}^2}{R_1k}\right)\bar{\eta}_1+\gamma\frac{1-\omega_1{}^2}{R_1k}\bar{\eta}_2=-\frac{1-\omega_1{}^2}{R_1k}\frac{P_0}{g}, \tag{2–1}$$

and

$$\frac{1-\omega_2{}^2}{R_2k}\bar{\eta}_1-\left(1+\frac{1}{\omega_2}+\frac{1-\omega_2{}^2}{R_2k}\right)\bar{\eta}_2=0, \tag{2–2}$$

where

$$\bar{\eta}_1=\rho_1\zeta_1+P_0/g,$$

and

$$\bar{\eta}_2=\rho_1\zeta_1+\Delta\rho\zeta_2+P_0/g,$$

and ζ_j is the displacement of the surface $j=1$ and the interface for $j=2$, P_0, ω and k are amplitude, nondimensional wave number and nondimensional frequency of the pressure disturbances, and $R_j=s_j/(s_1+s_2)$, respectively.

Solving equations (2–1) and (2–2), the $\bar{\eta}_j$'s are obtained as follows,

$$\bar{\eta}_1=\frac{(\delta P_0/g)\omega_1(1-\omega_1)\{R_2k+\omega_2(1-\omega_2)\}}{\{R_1k+\omega_1(1-\omega_1)\}\{R_2k+\omega_2(1-\omega_2)\}-\gamma\omega_1\omega_2(1-\omega_1)(1-\omega_2)}, \tag{2–3}$$

and

$$\bar{\eta}_2=\frac{(\delta P_0/g)\omega_1\omega_2(1-\omega_1)(1-\omega_2)}{\{R_1k+\omega_1(1-\omega_1)\}\{R_2k+\omega_2(1-\omega_2)\}-\gamma\omega_1\omega_2(1-\omega_1)(1-\omega_2)}, \tag{2–4}$$

or, in terms of nondimensional surface and interface displacements:

$$\tilde{\zeta}_1=\frac{\omega_1(1-\omega_1)\{R_2k+\omega_2(1-\omega_2)\}}{(\omega-\alpha_1)(\omega-\alpha_2)(\omega-\alpha_3)(\omega-\alpha_4)}-1, \tag{2–5}$$

and

$$\tilde{\zeta}_2=-\frac{\gamma}{\delta}\frac{R_2k\omega_1(1-\omega_1)}{(\omega-\alpha_1)(\omega-\alpha_2)(\omega-\alpha_3)(\omega-\alpha_4)}, \tag{2–6}$$

where α_j's are the frequncies of free waves of the system and defined as

$$|\alpha_i|<|\alpha_j| \text{ if } i<j, \text{ and } \tilde{\zeta}_j=\zeta_j/(P_0/\rho g),\ \gamma=\rho_1/\rho_2 \text{ and } \delta=\Delta\rho/\rho_2.$$

(A) $\omega=\alpha_1+\chi$

In the range of k, $1\gg k$ shown the smallest free frequency is expressed as follows:

$$\alpha_1\sim(R_1V_2+R_2V_1)k-R_1R_2k+\cdots\cdots, \tag{2–7}$$

and when the χ is much smaller than $|\alpha_1-\alpha_2|$, the nondimensional surface and interface displacements can be approximated as,

$$\tilde{\zeta}_1\sim-1+\delta\frac{(\chi-R_1k)(\chi+R_2k)}{k\chi}, \tag{2–8}$$

and

$$\tilde{\zeta}_2 \sim -\gamma \frac{R_2(\chi - R_1 k)}{\chi} . \tag{2- 9}$$

Further, in the case $|\chi| \gg \delta$ and $|\chi| \gg k$, the above relations become

$$\tilde{\zeta}_1 \sim -1 , \tag{2-10}$$

and

$$\tilde{\zeta}_2 \sim -R_2 + \frac{R_1 R_2 k}{\chi} , \tag{2-11}$$

which show the adjustment of the surface elevation is perfectly hydrostatic and the response of the system is nearly barotropic. On the other hand, when $\chi \ll \delta$ and $|\chi| \ll k$, that is, the waves are nearly equal to the free mode, $\omega \sim \alpha_1$, the hydrostatic adjustment can not hold and the response of the system becomes baroclinic as

$$\frac{\tilde{\zeta}_2}{\tilde{\zeta}_1} \sim -\delta^{-1} . \tag{2-12}$$

(B) $\omega = \alpha_2 + \chi$

In the same range of k as in (A), the free mode α_2 can be expressed as

$$\alpha_2 \sim 1 + (R_1 V_2 + R_2 V_1) k + R_1 R_2 k + \cdots\cdots , \tag{2-13}$$

which is baroclinic inertial mode as shown in section 1-(4). For the frequencies of disturbances near the free mode, that is, small values of χ, nondimensional forms of the displacements of the interface and surface will be approximated as

$$\tilde{\zeta}_1 \sim -1 + \delta \frac{\{R_1(R_2 - R_1)k + \chi\} \cdot \{R_2(R_2 - R_1)k - \chi\}}{k\chi} \tag{2-14}$$

and

$$\tilde{\zeta}_2 \sim -\gamma \frac{R_2\{R_1(R_2 - R_1)k + \chi\}}{\chi} . \tag{2-15}$$

These show the response of the system is nearly barotropic and the displacement of the surface is nearly static, when $|\chi| \gg k$, while, when $|\chi| \ll \delta$ and $|\chi| \ll k$, that is, when the deviation of the frequency is much smaller, expressions (2-14) and (2-15) become

$$\tilde{\zeta}_1 \sim \delta \frac{R_1 R_2 (R_2 - R_1)^2 k}{\chi} \tag{2-16}$$

and

$$\zeta_2 \sim -\gamma \frac{R_1 R_2 (R_2 - R_1) k}{\chi}, \tag{2-17}$$

which show the response of the system is baroclinic. The amount of the displacement of the surface differs very much from that for hydrostatic response.

Wave lengths of relatively small-scale atmospheric disturbances travelling along the south coast of Japan, are about ten degrees or less in longitude and their velocities are about ten degrees in longitude per day or 900–1000 km per day both from the analysis of Rossby waves on the surface of 700 mb and travelling speeds of lows (1965 to 1969) as shown in Table 3. From these, for example, disturbances of the wave length of about 500 km and 750 km have the periods of 1/2 and 0.75 days, respectively.

Considering the pressure effect only, the model used in this study can respond in a barotropic manner and the surface is displaced in a static manner for the real disturbance occurred near Japan.

Table 3. Travelling speeds of atmospheric disturbances.

	Jan.-March	April-June	July-Sept.	Oct.-Dec.	yearly
Low (1965–69)	1,085 km/day	1,075	910	1,000	1,015
*700 mb surface height	** 11.8 deg./day	10.4	8.0	9.9	10.0
	1,095 km/day	965	740	920	930

* Pettersen (1956), ** values at 30°N.

(II) *Effect of wind stress*

In the same way as in section (I), the equations corresponding to (2-1) become,

$$-\{R_1 k + \omega_1(1-\omega_1)\}\eta_1 + \gamma\omega_1(1-\omega_1)\eta_2 = -\frac{R_1 k}{g s_1}\frac{1-\omega_1}{1+\omega_1}(X - iY), \tag{2-18}$$

and

$$\omega_2(1-\omega_2)\eta_2 - \{R_2 k + \omega_2(1-\omega_2)\}\eta_1 = 0. \tag{2-19}$$

Solving the equations, we get

$$\eta_1 = \frac{\delta}{g}\Phi_0 \frac{\omega_1(1-\omega_1)\{R_2 k + \omega_2(1-\omega_2)\}}{\{R_1 k + \omega_1(1-\omega_1)\}\{R_2 k + \omega_2(1-\omega_2)\} - \gamma\omega_1\omega_2(1-\omega_1)(1-\omega_2)}, \tag{2-20}$$

and

$$\eta_2 = \frac{\delta}{g}\Phi_0 \frac{\omega_1(1-\omega_1)\cdot\omega_2(1-\omega_2)}{\{R_1k+\omega_1(1-\omega_1)\}\{R_2k+\omega_2(1-\omega_2)\}-\gamma\omega_1\omega_2(1-\omega_1)(1-\omega_2)}, \tag{2-21}$$

where $\Phi_0=k/\delta(s_1+s_2)\cdot(X-iY)/\omega_1(1+\omega_1)$, and X and Y are the x- and y-components of wind stress, respectively.

Comparing the expressions to those for pressure disturbance (2-3) and (2-4), the x-component of wind stress works in the same phase as pressure, and the y-component works with retardation of 90° when Φ_0 is positive or frequency ω is positive and larger than kV_1. In nondimensional forms the displacements of the surface and interface are expressed as follows:

$$\begin{aligned}\tilde{\zeta}_1 &= \frac{\zeta_1}{(X-iY)/\rho_1 g(s_1+s_2)} = \frac{\eta_1}{(X-iY)/g(s_1+s_2)} \\ &= \frac{k(1-\omega_1)\{R_2k+\omega_2(1-\omega_2)\}}{(\omega-\alpha_1)(\omega-\alpha_2)(\omega-\alpha_3)(\omega-\alpha_4)(1+\omega_1)}\end{aligned} \tag{2-22}$$

and

$$\begin{aligned}\tilde{\zeta}_2 &= \frac{\zeta_2}{(X-iY)/\rho_1 g(s_1-s_2)} = \frac{\eta_2-\eta_1}{(X-iY)/g(s_1+s_2)} \\ &= -\frac{\gamma}{\delta}\frac{R_2k^2(1-\omega_1)}{(\omega-\alpha_1)(\omega-\alpha_2)(\omega-\alpha_3)(\omega-\alpha_4)(1+\omega_1)}.\end{aligned} \tag{2-23}$$

(A) $\omega=\alpha_1+\chi$

When the frequency of disturbance comes near to the free mode α_1, the nondimensional expressions (2-22) and (2-23) can be approximated as follows:

$$\tilde{\zeta}_1 \sim \delta\frac{\{R_2k+(1-\chi)\chi\}(1-\chi+R_1k)}{\chi(1+\chi-R_1k)(1-\chi+2R_1R_2k)} \tag{2-24}$$

and

$$\tilde{\zeta}_2 \sim -\gamma\frac{R_2k(1+R_1k-\chi)}{\chi(1+\chi-R_1k)(1-\chi+R_1k)}, \tag{2-25}$$

or, if the deviation of the frequency χ is very small and $\chi \ll k$,

$$\tilde{\zeta}_1 \sim \delta\frac{R_2k}{\chi} \tag{2-26}$$

and

$$\tilde{\zeta}_2 \sim -\gamma\frac{R_2k}{\chi}. \tag{2-27}$$

In this range of ω, the response of the system to wind stress is baroclinic. When the deviation χ becomes a little larger and $1>\chi\gg k$, relations (2-24) and (2-25) become,

$$\zeta_1 \sim \delta \frac{1-\chi}{1+\chi} \tag{2-28}$$

and

$$\zeta_2 \sim -\gamma \frac{R_2 k}{\chi(1+\chi)} . \tag{2-29}$$

Therefore, the displacement of the surface ζ_2 depends on the wave length of the disturbance, and its sign depends on that of χ, the deviation of the frequency.

(B) $\omega = \alpha_2 + \chi$

In this case, expressions (2-22) and (2-23) become as follows:

$$\zeta_1 \sim \delta \frac{R_1 R_2 (R_2 - R_1)^2 k^2}{2\chi} \tag{2-30}$$

and

$$\zeta_2 \sim -\frac{R_1 R_2 (R_2 - R_1) k^2}{2\chi}, \tag{2-31}$$

for the range of χ very close to α_2 and $|\chi| \ll k$, and

$$\zeta_1 \sim -\delta \frac{\chi}{2+\chi} \tag{2-32}$$

and

$$\zeta_2 \sim -\gamma \frac{R_2 k}{(2+\chi)(1+\chi)} \tag{2-33}$$

for $|\chi| \gg k$. From this, the response of the system is not perfectly baroclinic except when the frequency is very close to the free mode α_2. The displacement of the surface is very small, and its sign depends on the deviation of frequency from the free mode α_2.

(C) $\omega = \alpha_j + \chi \quad (j = 3 \text{ or } 4)$

In case the frequency of the disturbance is near to the barotropic free modes of the system,

$$\alpha_j \sim \frac{1}{2} \pm \sqrt{\frac{1}{4} + \frac{k}{\delta}} \quad \text{for} \quad j = 3 \text{ or } 4,$$

expressions (2-20) and (2-21) can be approximated as

$$\zeta_1 \sim \frac{k}{2\chi\sqrt{\frac{1}{4} + \frac{k}{\delta}}} \tag{2-34}$$

and

$$\zeta_2 \sim \frac{\gamma R_2 k}{2\chi\sqrt{\frac{1}{4}+\frac{k}{\delta}}}, \qquad (2\text{-}35)$$

which show the response of the model is nearly barotropic.

Numerical examples of the response curve for wind stress for $k=0.01$ and 0.1 or wave length 10^3 km and 10^4 km are shown in Fig. 2. The atmospheric disturbances travelling along the south coasts of Japan shown in Table 3 have the period of about a day and the wave length of about 10^3 km on an average, while one of the free modes of the system simulating the sea south of Japan has the period of about a day or less, so the atmospheric disturbances travelling along the south coasts of Japan are apt to make large baroclinic changes of the sea condition if the parameters of the disturbance and those of the sea including the fundamental current system, density stratification, etc. match the above-mentioned resonance conditions.

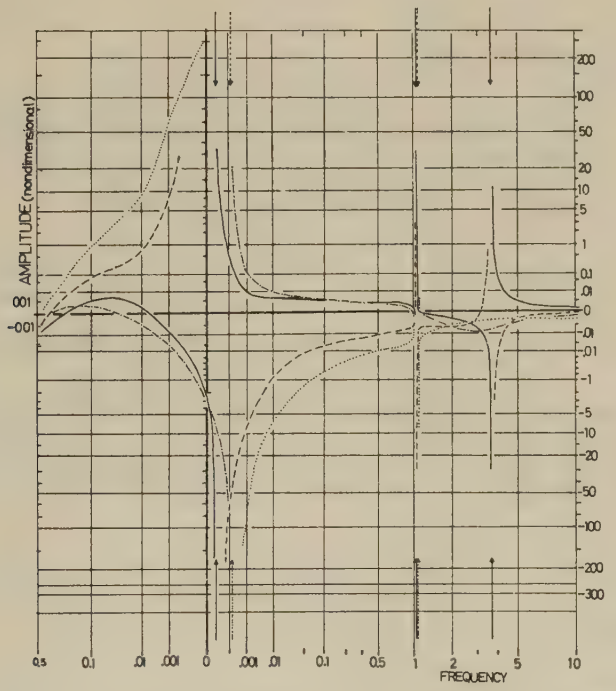

Fig. 2. Response of surface and interface for wind stress.
——— – – – – ($k=0.01$)
–·–·–·– ····· ($k=0.1$)
↓ Free mode for $k=0.01$ and ↓ for $k=0.1$

3. Free waves in the case when the Coriolis parameter or other parameters are not constant

In the case the Coriolis parameter, and the thickness of the layers and the depth of the system, depend on the distance from the coast, that is, functions of x, equation (2-24) in the previous paper (IIDA, 1970) becomes

$$\frac{d^2\eta_j}{dx^2} + A_j\frac{d\eta_j}{dx} + B_{j1}\eta_1 + B_{j2}\eta_2 + a_1\frac{d\eta_j}{dx} + b_{j1}\eta_1 + b_{j2}\eta_2 = 0, \tag{3-1}$$

where

$$\begin{aligned}
A_j &= \frac{\dot{h}_{0j}}{h_{0j}+\dot{h}_{0j}x},\\
B_{jj} &= -\left\{k^2 + \frac{f_0 k}{\sigma_{0j}}\frac{\dot{h}_{0j}}{h_{0j}+\dot{h}_{0j}x} + \frac{e_{0j}f_0 - {\sigma_{0j}}^2}{\delta g(h_{0j}+\dot{h}_{0j}x)}\right\},\\
B_{12} &= \frac{\gamma}{\delta}\frac{e_{01}f_0 - {\sigma_{01}}^2}{g(h_{01}+\dot{h}_{01}x)},\\
B_{21} &= \frac{1}{\delta}\frac{e_{02}f_0 - {\sigma_{02}}^2}{g(h_{02}+\dot{h}_{02}x)},
\end{aligned} \tag{3-2}$$

and

$$\begin{aligned}
a_j &= \left\{\frac{\ddot{h}_{0j}}{h_{0j}+\dot{h}_{0j}x} - \frac{1}{2}\frac{\dot{h}_{0j}\dot{h}_{0j}}{(h_{0j}+\dot{h}_{0j}x)^2}x\right\}x - \frac{e_{0j}\dot{f}_0 + f_0\dot{f}_0 + f_0\dot{V}_{0j} + 2\sigma_{0j}k\dot{V}_{0j}}{e_{0j}f_0 - {\sigma_{0j}}^2},\\
b_{jj} &= -\frac{k\dot{f}_0}{\sigma_{0j}} - \frac{kf_0}{\sigma_{0j}}\frac{e_{0j}\dot{f}_0 + f_0\dot{f}_0 + f_0\dot{V}_{0j} + 2\sigma_{0j}k\dot{V}_{0j}}{e_{0j}f_0 - {\sigma_{0j}}^2},\\
&\quad - \frac{kf_0\dot{h}_{0j}}{\sigma_{0j}(h_{0j}+\dot{h}_{0j}x)}\left(\frac{\dot{f}_0}{f_0} + \frac{k\dot{V}_{0j}}{\sigma_{0j}} + \frac{\ddot{h}_{0j}}{\dot{h}_{0j}} - \frac{1}{2}\frac{\ddot{h}_{0j}x}{h_{0j}+\dot{h}_{0j}x}x\right)x\\
&\quad - \frac{1}{\delta}\frac{fe_{0j} - {\sigma_{0j}}^2}{g(h_{0j}+\dot{h}_{0j}x)}\left(\frac{e_{0j}\dot{f}_0 + f_0\dot{f}_0 + f_0\dot{V}_{0j} + 2\sigma_{0j}\dot{V}_{0j}k}{e_{0j}f_0 - {\sigma_{0j}}^2} - \frac{1}{2}\frac{\ddot{h}_{0j}x}{h_{0j}+\dot{h}_{0j}x}\right)x,\\
b_{12} &= \frac{\gamma}{\delta}\frac{f_0e_{01} - {\sigma_{01}}^2}{g(h_{01}+\dot{h}_{01}x)}\left(\frac{e_{01}\dot{f}_0 + f_0\dot{f}_0 + f_0\dot{V}_{01} + 2\sigma_{01}\dot{V}_{01}k}{e_{01}f_0 - {\sigma_{01}}^2} - \frac{1}{2}\frac{\ddot{h}_{01}x}{h_{01}+\dot{h}_{01}x}\right)x,\\
b_{21} &= \frac{1}{\delta}\frac{e_{02}f_0 - {\sigma_{02}}^2}{g(h_{02}+\dot{h}_{02}x)}\left(\frac{e_{02}\dot{f}_0 + f_0\dot{f}_0 + f_0\dot{V}_{02} + 2\sigma_{02}\dot{V}_{02}k}{e_{02}f_0 - {\sigma_{02}}^2} - \frac{1}{2}\frac{\ddot{h}_{02}x}{h_{02}+\dot{h}_{02}x}\right)x,
\end{aligned} \tag{3-3}$$

for $j=1$ or 2, and

$$\begin{aligned}
h_j(x) &= h_0 - \dot{h}_{0j}x - \frac{1}{2}\ddot{h}_{0j}x^2 - \cdots\cdots,\\
f(x) &= f_0 + \dot{f}_0x + \cdots\cdots,
\end{aligned}$$

and

$$V_j(x) = V_{0j} + \dot{V}_{0j}x + \frac{1}{2}\ddot{V}_{0j}x^2 + \cdots\cdots \tag{3-4}$$

These equations are very complicated, so it is assumed that the motions can be divided perfectly into two regimes, barotropic and baroclinic, as mentioned in section 1-(7). For the baroclinic regime of motion, the system of single-layered ocean with the thickness of $h_1h_2/(h_1+h_2)$, mean current of $V_c=(R_2V_1+R_1V_2)$ and gravity of $g_c=\delta g$, can be used, while for the barotropic the system with the thickness of $h_t=h_1+h_2$, mean current of $V_t=(R_1V_1+R_2V_2)$ and gravity of $g_t=g$ can be used. By this assumption, the equations corresponding to (3-1) can be expressed in the same form both for the barotropic and baroclinic motions as follows:

$$\frac{d^2\eta}{dx^2}+A\frac{d\eta}{dx}+B\eta+a\frac{d\eta}{dx}+b\eta=0, \tag{3-5}$$

where

$$\begin{cases} A=\dfrac{\dot{h}_0}{h_0+\dot{h}_0x}, \\ B=-\left\{k^2+\dfrac{f_0k}{\sigma_0}+\dfrac{e_0f_0-\sigma_0^2}{g_0(h_0+\dot{h}_0x)}\right\}, \end{cases} \tag{3-5}$$

and

$$\begin{cases} a=\left\{\dfrac{\ddot{h}_0}{h_0+\dot{h}_0x}-\dfrac{1}{2}\dfrac{\dot{h}_0\ddot{h}_0}{(h_0+\dot{h}_0x)^2}x\right\}x-\dfrac{e_0\dot{f}_0+f_0\dot{f}_0+2\sigma_0\dot{V}_0k-f_0\ddot{V}_0}{e_0f_0-\sigma_0^2}, \\ b=-\dfrac{\dot{f}_0k}{\sigma_0}+\dfrac{f_0k}{\sigma_0}\dfrac{e_0\dot{f}_0+f_0\dot{f}_0+f_0\ddot{V}_0+2\sigma_0k\dot{V}_0}{e_0f_0-\sigma_0^2} \\ \quad -\dfrac{e_0f_0-\sigma_0^2}{g_0(h_0+\dot{h}_0x)}\left(\dfrac{e_0\dot{f}_0+f_0\dot{f}_0+f_0\ddot{V}_0+2\sigma_0\dot{V}_0k}{e_0f_0-\sigma_0^2}-\dfrac{1}{2}\dfrac{\ddot{h}_0x}{h_0+\dot{h}_0x}\right)x \\ \quad -\dfrac{kf_0\dot{h}_0}{\sigma_0(h_0+\dot{h}_0x)}\left(\dfrac{\dot{f}_0}{f_0}+\dfrac{k\dot{V}_0}{\sigma_0}+\dfrac{\ddot{h}_0}{\dot{h}_0}-\dfrac{1}{2}\dfrac{\ddot{h}_0x}{h_0+\dot{h}_0x}\right)x, \end{cases} \tag{3-7}$$

and $\sigma_0=\sigma-kV_{c0}$, $V_0=V_{c0}$, $h_0=h_c$, and $g_0=g_c$ for baroclinic motions, and $\sigma_0=\sigma-kV_{t0}$, $V_0=V_{t0}$, $h_0=h_t$ and $g_0=g_t$ for barotropic.

(I) *Coriolis parameter*

When only the Coriolis parameter is the function of x, equation (3-5) is expressed as

$$\frac{d^2\eta}{dx^2}+\frac{1}{x}\frac{d\eta}{dx}-\left\{k^2+\frac{f_0k}{\sigma_0}\frac{1}{x}+\frac{f_0^2-\sigma_0^2}{g_0s_0x}\right\}\eta$$
$$-2\frac{f_0\dot{f}_0+\sigma_0k\dot{V}_0}{f_0^2-\sigma_0^2}\frac{d\eta}{dx}+\left\{-2\frac{k\dot{f}_0}{\sigma_0}+2\frac{kf_0}{\sigma_0}\frac{f_0\dot{f}_0+k\sigma_0\dot{V}_0}{f_0^2-\sigma_0^2}-\frac{f_0k^2\dot{V}_0}{\sigma_0^2}\right\}\eta=0, \tag{3-8}$$

where some small terms are neglected, or in a nondimensional form:

$$D\eta-\lambda\eta+\varepsilon V\eta=0, \tag{3-9}$$

where

$$\lambda=\frac{1}{\omega}+\frac{1-\omega^2}{g_0\dot{h}_0k/f_0^2}, \qquad \varepsilon=\frac{2\dot{f}_0}{f_0k}, \qquad V=-cz\frac{d}{dz}+dz, \qquad K=\frac{g\dot{h}_0k}{\dot{f}_0^2},$$
$$c=\frac{1+\omega r}{1-\omega^2}, \quad r=\frac{k\dot{V}_0}{\dot{f}_0}, \quad d=-\frac{1}{\omega}+\frac{1+\omega r}{\omega(1-\omega^2)}-\frac{r}{2\omega^2} \quad \text{and} \quad \omega\fallingdotseq\frac{\sigma_0}{f_0}. \tag{3-10}$$

Putting $\xi=\nu z$ and $\eta'=e^{\alpha z}\eta$, the equation is changed into

$$\xi\frac{d^2\eta'}{d\xi^2}+\frac{d\eta'}{d\xi}-(\xi+\Lambda)\eta'=0 \tag{3-11}$$

with the boundary conditions η or η' are finite both as ξ approaches to 0 and infinity, where $\nu^2=1-\varepsilon d+\varepsilon^2c^2/4$, $\alpha=-\varepsilon c/2$ and $\Lambda=(\lambda-\varepsilon c/2)/\nu$. Then solutions of equation (3-11) can be expressed in terms of Laguerre polynomials:

$$\eta\propto e^{-k(\nu-\varepsilon a/2)x}\cdot L_n(2k\nu x) \tag{3-12}$$

with the following characteristic equation:

$$\frac{1}{\omega}+\frac{1-\omega^2}{K}=-(2n+1)\sqrt{1-\varepsilon d+\frac{1}{4}\varepsilon^2c^2}+\frac{1}{2}\varepsilon c, \tag{3-13}$$

which is approximated, when ε is very small, as follows:

$$\omega^3-(1+NK)\omega-K\sim\frac{1}{4}\frac{\varepsilon K}{\omega(\omega^2-1)}\{2(N+r)\omega^3+(2+3rN)\omega^2-rN\}, \tag{3-14}$$

where $N=2n+1$,

$$\varepsilon=\frac{2\dot{f}_0}{f_0k}, \qquad K=\frac{g_0s_0k}{f_0^2}, \qquad \omega=\frac{\sigma_0}{f_0}, \quad \text{and} \quad \sigma_0=\sigma-kV_0.$$

The correction terms for the free mode frequencies of the system where the Coriolis parameter is constant are

$$\varepsilon_j\sim\frac{1}{2}\varepsilon\frac{K\tilde{\omega}_j(N\tilde{\omega}_j+1)}{(\tilde{\omega}_j^2-1)\{3\tilde{\omega}_j^2-(1+NK)\}}, \tag{3-15}$$

where $\tilde{\omega}_j$ is a root of the following equation:

$$\tilde{\omega}_j^3-(1+NK)\tilde{\omega}_j-K=0, \tag{3-16}$$

which is the characteristic equation for the constant Coriolis parameter. When K is small compared with unity, the following approximations of the roots of equation (3-16) will hold:

$$\tilde{\omega}_j \sim \begin{cases} 1+(n+1)K, & j=1, \\ -(1+nK), & j=2, \\ -K, & j=3, \end{cases} \tag{3-17}$$

Using the relations, correction terms (5-2. 8) become

$$\varepsilon_1 \sim \frac{1}{4}\varepsilon \frac{2+(4n+3)K}{2+(4n-5)K},$$

$$\varepsilon_2 \sim \frac{1}{4}\varepsilon \frac{2+(4n+1)K}{2+(4n-1)K},$$

and

$$\varepsilon_3 \sim -\frac{1}{2}\varepsilon \frac{K^2(1-NK)}{1+NK}. \tag{3-18}$$

From these expressions, the corrections for barotropic waves are very small (1 to 2% for the wave length of about 5,000 km), while those for baroclinic become important from the wave length of 700 to 1,000 km, and reach about 20% for the wave length of about 5,000 km except for ε_3.

(II) *Bottom and interface profiles*

In case only the bottom, interface and surface profiles are functions of x and proportional to each other, equation (3-7) becomes

$$\frac{d^2\eta}{dx^2}+\frac{1}{x}\frac{d\eta}{dx}-\left(k^2+\frac{kf_0}{\sigma_0}\frac{1}{x}+\frac{f_0^2-\sigma_0^2}{g_0 s_0 x}\right)\eta - \\ -\frac{\tau_0}{2s_0}\left\{\frac{d\eta}{dx}-\left(\frac{kf_0}{\sigma_0}+\frac{f_0^2-\sigma_0^2}{gs_0}\right)\eta\right\}=0, \tag{3-19}$$

where the depth is assumed to change as $h=h_0(1-e^{-lx})$ or $h=h_0lx-h_0l^2x^2/2+\ldots$, and $\tau_0=h_0l^2$ and $s_0=h_0l$. In a nondimensional form, the above equation is expressed as

$$z\frac{d^2\eta}{dz^2}+\frac{d\eta}{dz}-\left(z+\frac{1}{\omega}+\frac{1-\omega^2}{K}\right)\eta-\frac{\tau_0 z}{2s_0 k}\left\{\frac{d}{dz}-\left(\frac{1}{\omega}+\frac{1-\omega^2}{K}\right)\right\}\eta=0. \tag{3-20}$$

By the same procedures as in the previous section (I), the following characteristic equation is obtained.

$$\frac{1}{\omega}+\frac{1-\omega^2}{K}-\frac{1}{2}\varepsilon c=-(2n+1)\sqrt{1-\varepsilon d+\frac{1}{4}\varepsilon^2 c^2}, \tag{3-21}$$

where $\varepsilon=\tau_0/2s_0k=l/2k$, $c=1$, and $d=1/\omega+(1-\omega^2)/K$. When ε is small or the scale of the change of the depth, etc., l, is small compared with wave length k, the above

equation is approximated as

$$\omega^3-(1+NK)\omega-K\sim\frac{1}{2}\varepsilon\{N\omega^3-(N+K)\omega-NK\} \tag{3-22}$$

and the correction terms become

$$\varepsilon_j\sim\frac{1}{2}\varepsilon\frac{K(N^2-1)\tilde{\omega}_j}{3\tilde{\omega}_j^2-(1+NK)}, \tag{3-23}$$

where $\tilde{\omega}_j$, K and N are defined as in the previous case. When K is small, substituting the roots (5–2. 10) into relation (5–2. 16), ε_j can be expressed in the following form:

$$\varepsilon_1\sim\frac{1}{2}\varepsilon\frac{(N^2-1)\{1+(n+1)K\}K}{2+(4n-5)K},$$

$$\varepsilon_2\sim-\frac{1}{2}\varepsilon\frac{(N^2-1)(1+nK)K}{2+(4n-1)K},$$

and

$$\varepsilon_3\sim\frac{1}{2}\varepsilon\frac{(N^2-1)K^2}{1+NK}. \tag{3-24}$$

which show the corrections for baroclinic waves are smaller than for barotropic.

4. Concluding remarks

The free waves in a two-layered rotating sea with variable depth and fundamental current system are treated in the previous paper. In this paper, the response of the system to periodic atmospheric disturbances propagating along the coast are considered, at first. Then, in section 3, the effect of the variability of the Coriolis parameter and inclinations of the surface and interface with the distance from the coast are discussed.

The system can respond mostly in a barotropic manner and the surface displacement is almost hydrostatic to atmospheric pressure, except when the frequency of the disturbance is very close to those of the baroclinic free modes. For wind stress the system responds baroclinically near the frequencies of the baroclinic free modes and barotropically near those of the barotropic ones. In the frequency ranges between those of the free modes, the response is rather complicated. Especially for the ranges of frequency between barotropic and baroclinic free modes, the displacement of the surface has the same sign as that of the interface, and much smaller than the latter.

The β-correction is, generally, larger for baroclinic than for barotropic in the same values of wave number. In case $d^2h/dx^2 \neq 0$, the effect is larger for barotropic than for baroclinic.

Acknowledgement

The author wishes to thank professors Kozo YOSHIDA and Kinjiro KAJIURA for their useful advice.

References

IIDA, H. (1970): Edge waves on the linearly sloping coast-I Free waves. *Oceanogr. Mag.*, **22**, 37–62.

KAJIURA, K. (1958): Effect of free and forced waves. *J. Mar. Res.*, **16**, 145–157.

REID, R.O. (1958): Effect of Coriolis force on edge waves (I). *J. Mar. Res.*, **16**, 109–144.

YOSHIDA, K. (1960): The oceanic waves of days to months periods. *Records Oceanogr. Works Japan*, **5**, 11–24.

一様に傾斜した海岸におけるエツヂ・ウエーブ

II 強制波と β 効果等

飯　田　隼　人

（気象庁・海洋気象部）

前回（飯田，1970）に引きつづき，一様に傾斜した海底を持つ直線上の海岸に沿って伝わるエッヂ・ウエーブの問題のうち，周期的に海岸線に平行に移動する気象擾乱に対する応答問題，および自由波に対する β 効果や深さの変化が一様でないことによる効果を調査した．気象擾乱は気圧，風のストレスの x および y 成分に分けてそれぞれ考察した．β 効果については海岸が東西にのびているものとした．深さの変化については $d^2h/dx^2 \neq 0$ をパラメーターとして考えた．

The Oceanographical Magazine
Vol. 24, No. 1, pp. 57 to 63, December 1972

The mean sea surface temperature of the Okhotsk Sea in cooling season (Second report)

——Normal sea surface temperature——

Masaomi AKAGAWA

Hakodate Marine Observatory

(Received September 9, 1972)

Abstract. The normal sea surface temperatures of the Okhotsk Sea in the cooling season were drawn by the present author in 1968 from the data of U.S.S.R. maritime meteorological broadcast during the years 1960–1965. However, the charts are unsatisfactory because the statistical period of the six years is too short to represent the normal sea surface temperature.

Here, new charts are prepared by using the data from 1960 to 1970. That is, the recent data of the five years 1966–1970 are added. Though there is not a great difference in the pattern between the two series, the new mean sea surface temperatures are somewhat lower in the greater part of the sea than the old ones.

The change of the air temperature shows the same tendency as that of the sea surface temperature, and the pack ice appears earlier in the latter period (1966–1970) than in the former years (1960–1965) on an average.

1. Introduction

A set of charts of the normal 5-day mean sea surface temperature of the Okhotsk Sea in the cooling season, that is, from October to December, was presented in the previous paper by the present author (AKAGAWA, 1968). The statistics were taken from the charts of the 5-day mean sea surface temperature during the years 1960–1965 prepared by the Marine Division of the Japan Meteorological Agency on the basis of the data from the U.S.S.R. maritime meteorological broadcast.

In the previous paper, the roles of the extension of the Sōya Warm Current, the southward flow of the East Saghalien Current, and the cold sea area in the neighbourhood of the central Kurile Islands were discussed. In paticular, the retardation of falling of the sea surface temperature in November was pointed out, and in this connection, the effects of the cyclone tracks and the vertical structure of the water temperature in the mixing layer were discussed. It was also pointed out that the transition of 0°C isotherm is related to the expansion of the ice area.

However, the statistical period of the six years is too short for indication of the normal sea surface temperature, so the new statistics are made from the data from 1960 to 1970. The data of the recent five years (1966–1970) are added, so the data of eleven years are available, though the data of October in 1970 are missing. The method of statistics is the same as that in the old statistics. In the cooling season the so-called thermohaline convection develops and ice formation begins in the Okhotsk Sea, so the oceanographic conditions are very changeable. The new normal sea surface temperature is prepared to be available for various studies.

2. Comparison between the new and the old statistics

The new normal sea surface temperatures are shown in Fig. 1. There are little differences in the normal pattern between the new charts and the old ones. The differences of the sea water temperature at each point are less than 0.3°C in the most part of the Okhotsk Sea, but are nearly 1°C at the border of the sea. Characteristic features in the distribution of these differences are as follows:

October; In the beginning of the month the new statistics show generally lower temperature than the old ones and the sea area with this feature shifts eastward becoming narrower, and the higher temperature areas extend southward from the northern part of the Okhotsk Sea. The new statistics show lower temperature in the southern part of the Okhotsk Sea and higher temperature around the central part of the Kurile Islands.

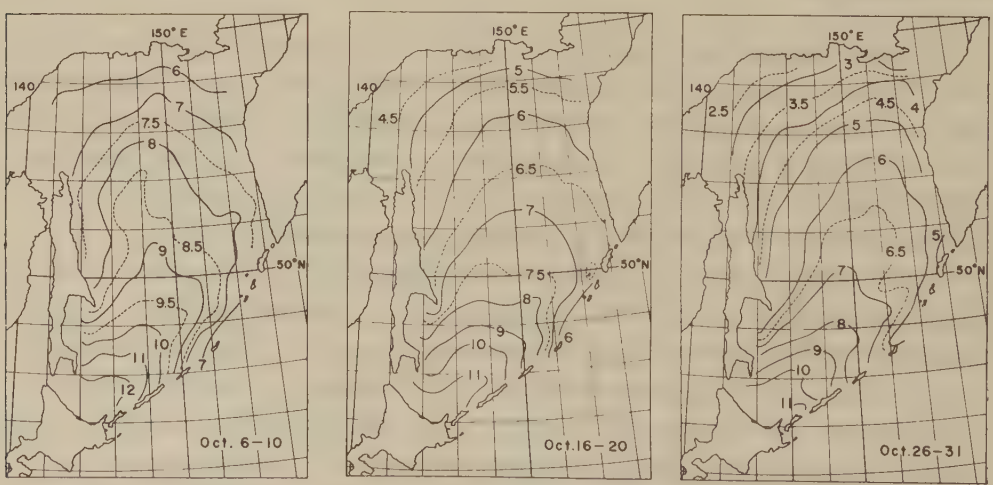

(a) (b) (c)

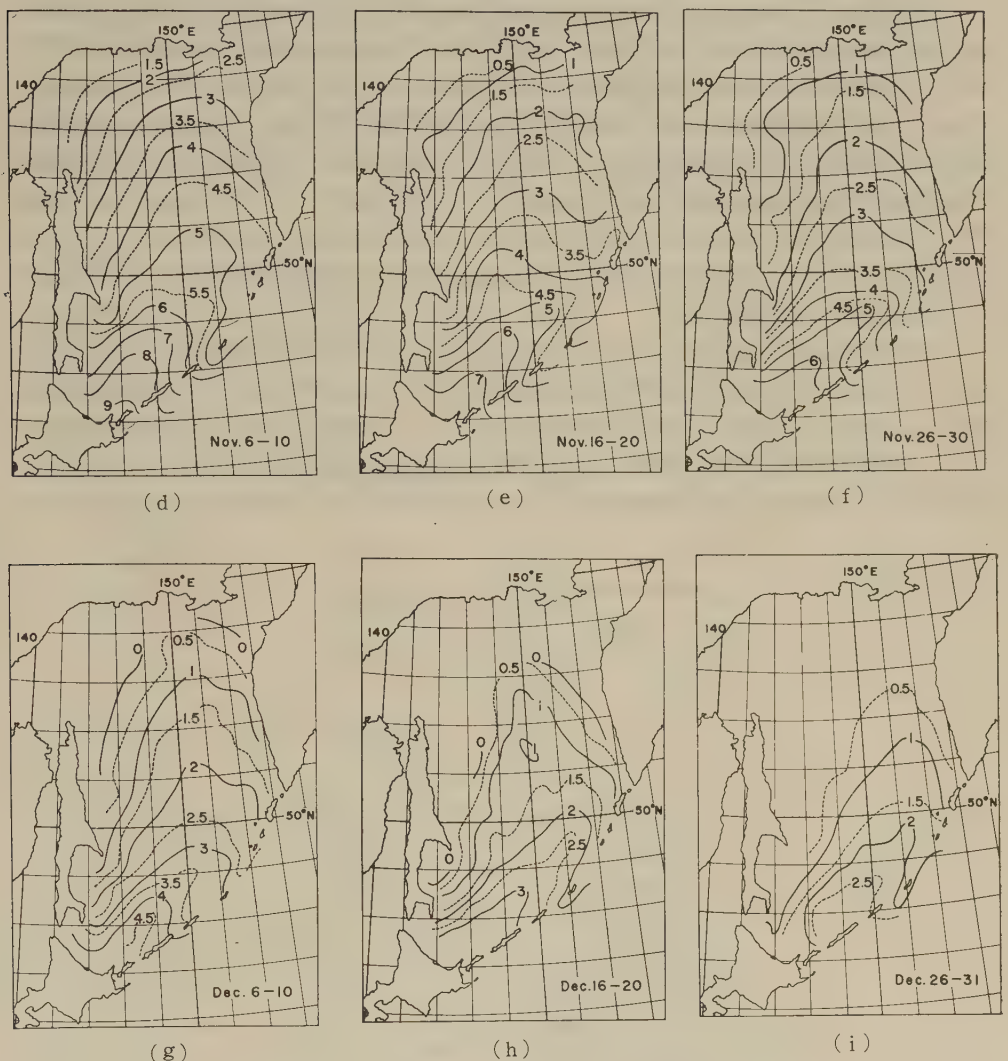

Fig. 1. Normal sea surface temperature (°C).

November; The new statistics show higher temperature near the northern part of the Kurile Islands. It is remarkable that the new normal values are higher near the northern part of the Okhotsk Sea at the beginning of the month and become lower on the whole at the end of the month.

December; The new statistics show generally higher temperature in the western and southern parts of the Okhotsk Sea.

The mean differences of the sea surface temperature through this season between the two statistical values are shown in Fig. 2. The maximum difference is 0.3°C, and the new values show the higher temperature in the border part and somewhat lower in the central part of the Okhotsk Sea than the old ones. It may be possible that this means the warming of the East Saghlien Current Water and the decay of northeastward expansion of the southern warm water in the Okhotsk Sea since 1966. However, the data on the border part of the sea become scarce as the formation of sea ice advances, so the effect of the unevenness of the statistical data should be taken into consideration.

Analyses were made on the air temperature and the data when the pack ice began to appear. Table 1 shows the examples of the variation of the air temperature at coastal stations of the Okhotsk Sea. It is evident that the air temperature in the cooling season was lower during the years 1966–1970 than that in the years 1960–1965 as well as the tendency of changing of the sea surface temperature. It

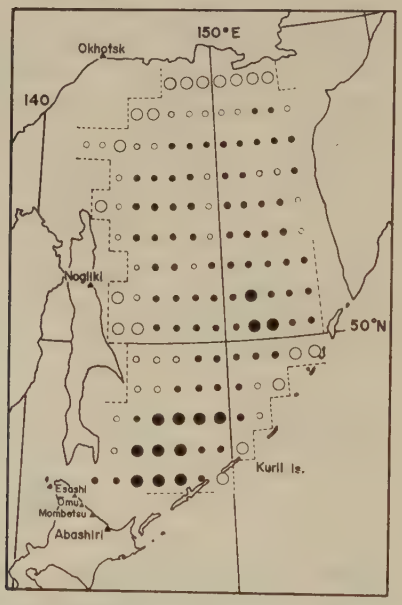

Fig. 2. Differences of the mean sea surface temperature between the new statistics (1960–1970) and the old ones (1960–1965).
○: +0.2—+0.3°C, ○: +0.0—+0.1°C } The new values are higher than the old ones,
●: −0.0—−0.1°C, ●: −0.2—−0.3°C } the new values are lower than the old ones.

Table 1. Changes of the mean air temperature at the coastal stations of the Okhotsk Sea (°C).

Station, Season \ Periods	1960–'65	1966–'70	Data Remarks
at Okhotsk, in Dec.-Feb.	−20.0	−21.6*	after YAMAZAKI (1971)
at Nogliki, in Nov.	− 8.7**	− 9.2**	from U.S.S.R. coastal hydrographic broadcasting
at Abashiri, in Oct.-Dec.	3.5	3.4	

*: the mean value in the period from 1966 to 1969,
**: the mean values observed at 18 GMT.

Table 2. The mean date when the pack ice began to appear at the Okhotsk coasts of Hokkaido.

Period \ Station	Kitamiesashi	Ōmu	Mombetsu	Abashiri
1961–1966 mean	Jan. 20	Jan. 19	Jan. 18	Jan. 17
1967–1971 mean	Jan. 13	Jan. 14	Jan. 15	Jan. 13
1961–1971 mean	Jan. 17	Jan. 17	Jan. 17	Jan. 15

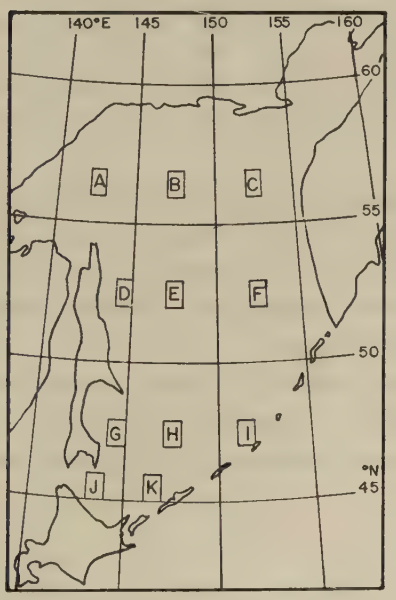

Fig. 3. Positions of the selected sea regions.

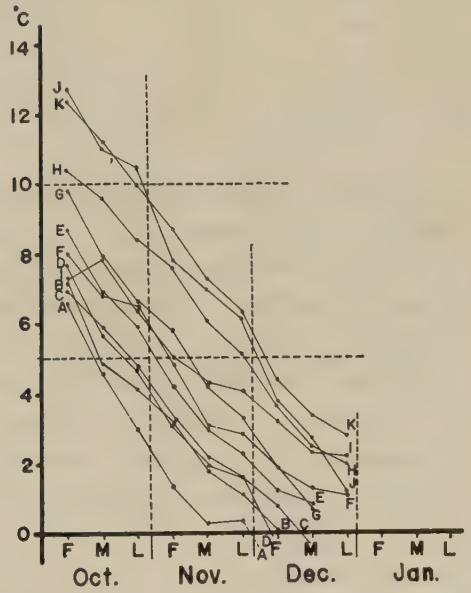

Fig. 4. Changes of the sea surface temperature in the selected sea regions.

is clear from Table 2 that the pack ice began to appear about five days earlier in the period 1967–1971 than in the years 1961–1966 on an average.

Here, synthesizing these statistical results, it is reasonable to say that the sea surface temperature in the cooling season was generally lower during the years 1966–1970 than in the years 1960–1965.

3. Changes of the sea surface temperature

The changes of the sea surface temperature in the selected sea regions shown in Fig. 3 are illustrated in Fig. 4, and the mean differences are given in Table 3.

Table 3. Differences of the ten-day mean sea surface temperature in the selected sea regions (°C/10-days). In the column of period the letters denote as follows: F; the beginning, M; the middle, and L; the end of a month respectively.

Region / Period	A	B	C	D	E	F	G	H	I	J	K	Mean
Oct. F—Oct. M	−2.0	−1.4	−1.1	−2.0	−1.8	−1.2	−1.8	−0.8	+0.6	−1.7	−1.2	−1.3
Oct. M—Oct. L	−1.6	−1.7	−1.1	−1.0	−1.0	−0.3	−1.4	−1.2	−1.5	−0.5	−1.2	−1.1
Oct. L—Nov. F	−1.6	−0.9	−1.5	−1.6	−1.7	−1.7	−0.8	−0.8	−1.4	−2.7	−1.3	−1.5
Nov. F—Nov. M	−1.1	−1.4	−1.1	−1.2	−1.2	−1.7	−1.6	−1.5	−0.7	−0.8	−1.4	−1.2
Nov. F—Nov. L	+0.1	−0.7	−0.6	−0.3	−0.7	−0.2	−0.9	−1.0	−0.2	−0.8	−1.0	−0.6
Nov. L—Dec. F	?	−1.0	−0.8	−1.8	−1.0	−1.0	−1.4	−1.4	−0.9	−2.4	−1.9	−1.4
Dec. F—Dec. M	?	?	−1.1	?	−0.4	−0.6	−1.1	−1.2	−0.8	−1.1	−1.0	(−0.9)
Dec. M—Dec. L	?	?	?	?	?	−0.2	?	−0.5	−0.2	−1.5	−0.6	(−0.6)

The features of changes of the sea surface temperature in the new statistics do not differ from those in the old ones. The falling ratio of the sea surface temperature in the period from the middle to the end of November is noticeable as pointed out in the previous paper. The falling ratio in that period is about 0.6°C/10-days which is a half of the ratios in the earlier and the later periods.

In this connection, the effects of the different tracks of cyclones in November and the vertical structure of the water temperature influencing to the change of the sea surface temperature by convectional mixing process were discussed in the previous paper (AKAGAWA, 1968).

Acknowledgement

The author wishes to express his deep thanks to the members of the Marine

Meteorological Division of the Japan Meteorological Agency who prepared the charts of the 5-day mean sea surface temperature, and to Dr. Kn. WATANABE of the Kyoto Gakuen University for his valuable advices.

This work was partially supported by the Japan Society for Promotion of Science as a part of the United States-Japan Cooperative Science Programme (4R-005).

References

AKAGAWA, M. (1968): The mean sea surface temperature of the Okhotsk Sea in cooling season (Preliminary report). *Records Oceanogr. Works Japan*, **9**, 263–278.

YAMAZAKI, M. (1971): Long-range forecasting for occurrence of cold winter in North Japan. *Manual of seasonal weather forecasting in Japan, JMA*, **1**, p. 201, Fig. 9.22.

冷却期におけるオホーツク海の平均海面水温（第2報）

―― 新しい水温分布図 ――

赤　川　正　臣

（函館海洋気象台）

著者は先に気象庁海洋気象部作成の 1960～'65 年の 10～12 月におけるオホーツク海の半旬平均水温図（ソ連海上実況気象報の資料による）から緯・経度1度ますごとの平均水温を算出し，それによる6年間の平均水温分布図を作った．

しかし，6年間の平均では平年値として扱うには統計期間が短か過ぎるので，新たにその後の 1966～'70 年の資料を加えて，1960～'70 年の最大11年間の資料によって再統計し新しい水温分布図を作った．

この新・旧分布図を比較すると，水温分布のパターンはほとんど変りがなく，11月における水温降下の鈍化現象は新統計にも現われているが，新統計の方が全体的にやや低温の結果となった．

ちなみに，1966～'70 年と 1960～'65 年との 10～12 月の気温を比較すると，前者の期間のほうが低温であり，対応する年々の北海道オホーツク海沿岸の流氷初日も平均すると前者のほうが早くなっている．

The Oceanographical Magazine
Vol. 24, No. 1, pp. 65 to 79, December 1972

On the distribution of phosphorus along 170°W longitude in the Pacific and Antarctic Oceans

Hirozo YOSHIMURA

Japan Meteorological Agency

(Received September 20, 1972)

Abstract: The distribution of phosphorus obtained in The Southern Cross Cruise of the *Hakuho-Maru* (Nov. 1968 – Mar. 1969) is as follows:

(1) In the phosphorus profile along 170°W longitude, the contents of phosphate-phosphorus in the intermediate and deep waters increase toward north except in the Ross Sea.

(2) There are two rich areas of organic phosphorus along 170°W longitude. One is found in the Antarctic convergence region, and another in the Equatorial Current zone.

(3) The surface waters at tropical and subtropical regions show high ratios of organic phosphorus to total phosphorus. This phenomenon seems to be due to the biological uptake of phosphate-phosphorus under the high water temperature and strong insolation in the Torrid Zone.

1. Preface

During the Southern Cross Cruise, the data for phosphate-phosphorus and total phosphorus were obtained aboard the *Hakuho-Maru* from surface to bottom in the central and southern Pacific along 170°W longitude as far as the Antarctic. Measurements of phosphate-phosphorus were made at all stations of hydrographic cast and those of total phosphorus at 24 stations at intervals of 3°–6° latitude.

The author's purpose of the investigation in the Southern Cross Cruise was to clarify the distribution of phosphorus in relation to other hydrographical elements, *viz.*, dissolved oxygen, AOU, water temperature and salinity.

2. Method of analysis

As an analytical method for phosphate-phosphorus, the reduction of phosphomolybdate-complex by using stannous chloride was done. The absorbance of reduced phosphomolybdate-complex was measured about 15 minuites after addition of

stannous chloride solution. On the other hand, for the analysis of total phosphorus, reduction by ascorbic acid was done and the measurment of absorbance was made by photo-electric photometer with the wave length of 700 mμ about 40 minuites after the reagents being added.

To liberate phosphate-phosphorus from organic matter, the oxidation method using potassium persulfate (MENZEL, 1965) was employed. In this method, arsenic which interferes the measurement of total phosphorus is not removed. Consequently, the correction for arsenic is neccessary. The contribution by arsenic may be estimated in the comparision of optical absorbance at the wave length of 700 mμ between phosphomolybdate-complex and arsenomolybdate-complex, and derived from arsenite and arsenate in sea water.

Based on the above-mentioned fact, the contribution by arsenite was corrected for the data of total-phosphorus, because the contents of arsenite only have an effect on the measurment values of organic phosphorus. The arsenite, being changed to arsenate in oxydation process, fairly contributes to the values of organic phosphorus obtained by the subtraction of phosphate-phosphorus from the total phosphorus in the intermediate and deep waters. On the other hand, the contribution of arsenate is cancelled by the subtraction of phosphate-phosphorus from total phosphorus. The values of arsenite concentration described by KANAMORI, *et al.* (1968) and other KANAMORI's memoir was employed for the correction of organic phosphorus.

According to the author's test by photometry, the optical absorbance of arsenate is 0.75 of that of phosphate in the wave length of 700 mμ. The concentration of arsenite is mostly less than 0.5 μg/l above about 600 m depth, but it is 0.7 μg/l on an average in the intermediate and deep waters below 600 m depth in the Pacific. Accordingly, the subtraction as much as 0.01 μg-atom/l was carried out to the values of total phosphorus below 600 m depth.

The influence of silicomolybdate-complex can not be disregarded when ascorbic acid is used. Therfore, the author carried out a correction employing the method of SUGAWARA *et al.* (1968). According to this method, the correction value of silicomolybdate-complex is given in the range of 0.00–0.03 μg-atom/l depending on the concentrations of silicate and phosphate, and the values are subtracted from the values of total phosphorus.

3. Distribution of phosphorus

*3–1. Distribution of inorganic phosphate-phosphorus along 170°W and 155°E longitudes**

The profiles of inorganic phosphate-phosphorus along 170°W and 155°E are shown in Figs. 1 and 2. The distribution of phosphate in the area under consideration has a maximum in the lower part of the intermediate water with low salinity, except the Antarctic area occupying the south from about 50°S latitude along 170°W longitude. This maximum layer appears at 700 m to 1,500 m depth at the northern part and at 1,200 m to 2,000 m depth at the southern part. And the phosphate concentration in the maximum layer remarkably increases to the north, particularly in the North Pacific.

Comparing with the profile on 170°W meridian, the maximum region having a center in the North Pacific somewhat expands to farther south on 160°W (REID,

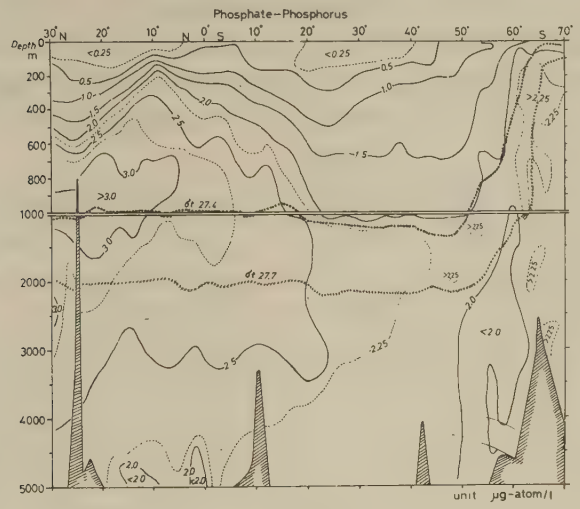

Fig. 1.

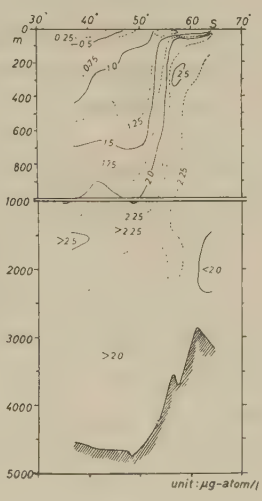

Fig. 2.

Fig. 1. Profile of inorganic phosphate-phosphorus along 170°W between 30°N and 69.5°S.

Fig. 2. Profile of inorganic phosphate-phosphorus along 155°E between 63°S and 38°S.

* Quoted from "Preliminary Report of the *Hakuho-Maru* Cruise KH-68-4" and "Oceanographical Data of KH-68-4 of the *Hakuho-Maru*".

1965) and 140°W meridians (SAPOZHNIKOV and MAKIEVSKAYA, 1966). But comparing with the meridian of 170°E (SAPOZHNIKOV and MAKIEVSKAYA, 1966), the maximum region on 170°W meridian expands to the south.

The phosphate concentration in the maximum layer increases toward the northeast of the Pacific. Such a remarkable increase of phosphate concentration in the maximum layer mentioned above in the Pacific can not be seen in other oceans. In the Indian Ocean, the increase in the maximum layer is slight as far as the Arabian Sea and the Gulf of Bengal. And in the Atlantic, its tendency can not be recognized in the northeastern side of the ocean. Consequently, the remarkable increase of phosphate concentration in the maximum layer is a characteristic in the distribution of phosphate in the Pacific (REDFIELD, 1960).

In the surface waters above 100 m depth in the Tropical, Subtropical and Equatorial regions along 170°W longitude, the contents of phosphate-phosphorus have a range of 0.00–0.10 μg-atom/l. However, the contents in the Antarctic and Sub-Antarctic regions exceed 1.0 μg-atom/l. The contents of phosphate-phosphorus in the deep water and the bottom water show a gradual increase from the Antarctic deep water contains about 2.0 μg-atom/l of phosphate-phosphorus, but the North Pacific deep water shows the contents of 2.5 μg-atom/l along 170°W longitude.

The phosphate-phosphorus distributed along 155°E longitude also has a maximum which slightly exceed 2.25 μg-atom/l at the depth of a little beyond 1,000 m.

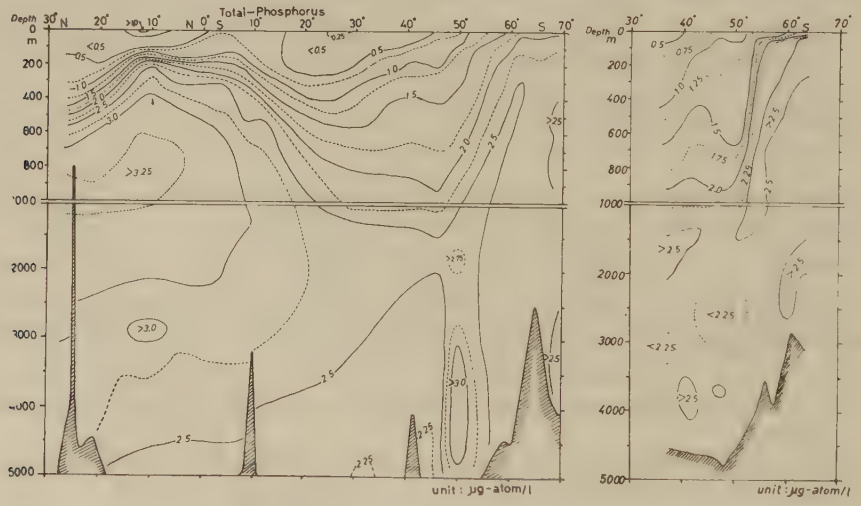

Fig. 3 Fig. 4.

Fig. 3. Profile of total phosphorus along 170°W between 30°N and 69.5°S.
Fig. 4. Profile of total phosphorus along 155°E between 63°S and 38°S.

*3-2. Distribution of total phosphorus along 170°W and 155°E longitude**

The profiles of total phosphrus along 170°W and 155°E are shown in Figs. 3 and 4. The profile of total phosphorus has a similarity with that of inorganic phosphate-phosphorus which is described in the previous section. For example, the profile of total phosphorus also shows a maximum in the lower part of the intermediate layer and the concentration has an increasing tendency to the north along 170°W longitude. On the other hand, in the Sub-Antarctic region, very high contents of total phosphorus are found in the intermediate and deep waters. The intermediate water of the Pacific originates in the upper layer water penetrating from about 62°S latitude, and this penetration is shown by the maximum layer of total phosphorus in Fig. 3.

On the profile of 155°E longitude, the maximum in the Sub-Antarctic region also is shown by a pattern with a tongue of penetration.

3-3. Distribution of inorganic phosphate-phosphorus and total phosphorus related with the other oceanographical elements

a) The maximum layer of phosphate-phophorus approximately occupies the zone between 6°C and 2°C isothermes. In the upper layers, isothermes of 20°C and 10°C roughly coincide with the lines expressing the phosphate concentration of 0.5 μg-atom/l and 1.0 μg-atom/l respectively.

b) The depth of the inorganic phosphate maximum (generally 700 m–2,000 m) corresponds approximately to the depth of lower margin of the salinity minimum tongue. The salinity minimum occupying the upper margin of phosphate minimum tongue shows the values between 34.0‰ and 34.6‰.

The salinity minimum in the northern intermediate water penetrates to the area around 10°N latitude in the Tropical region, and this water upwells to 100 m depth near 10°N. On the other hand, the salinity minimum water sinking from the surface around 62°S latitude in the southern hemisphere penetrates as far as 5°S latitude. The salinity at the minimum layer in the southern hemisphere increases with depth toward north, and the final value reaches 34.4‰ or more at about 800–1,000 m depth.

In the north Tropical region, a remarkable transition layer of phosphate-phosphorus exists between the surface and the intermediate waters. This transition layer coincides with the transition layer of salinity and temperature. The vertical gradient of phosphate concentration is 2.6×10^{-4} μg-atom/l/cm at 93–140 m depth at

* Quoted from "Preliminary Report of the *Hakuho-Maru* Cruise KH-68-4".

St. 16 (9°N, 170°W).

c) Dissolved oxygen and pH profiles along the 170°W and 155°E longitude have approximatly a similarity to the phosphate profile. Namely, the increase of dissolved oxygen and pH corresponds to the decrease of phosphate, and *vice versa*. Nevertheless, the minima of the dissolved oxygen and pH appear at the shallower depth than the layer of the phosphate maximum in the north Tropical region.

According to "The Preliminary Report of the *Hakuho-Maru* Cruise KH-68-4", dissolved oxygen contents in the minimum layer in the southern hemisphere along the meridian of 170°W ranges from 2.9 to 4.1 *ml/l* except the regions north of 9°S and south of 64°S. The oxygen-minimum layer occupies the lower part of the intermediate water.

pH minimum on the meridian of 170°W shows the values below 7.7 in the north Tropical region and 7.8–7.9 in the south hemisphere.

d) The σ_t of the phosphate-phosphorus maximum layer fluctuates in the northern regions along 170°W longitude. In the sinking area of the southern hemisphere, the phosphate maximum layer coincides with the surface of σ_t 27.7. On the other hand, phosphate maximum layer corresponds with the different surface of σ_t in the northern hemisphere. A correspondence of the phosphate maximum and the surface of σ_t 27.4 is found out in the area near 10°N, as indicated by SAPOZHNIKOV and MAKIEVSKAYA (1966). However, in the Equatorial and Tropical regions, the phosphate maximum moves to the surface of σ_t less than 27.4.

4. Phosphate-phosphorus in the surface water

For the purpose of making clear the regional distribution of phosphorus, the total amounts of phosphorus contained in the surface layer (0–100 m depth) along the meridian of 170°W is shown in Fig. 5. In Fig. 5, the total amounts of phosphate-phosphorus and organic phosphorus are shown with a solid line and a broken line respectively. The total amounts of phosphate-phosphorus have two peaks in the Antarctic region and the Tropical-Equatorial regions. The peak of the Antarctic region which is due to vertical mixing with deeper water in winter shows a very large value as compared with that of the other regions. The secondary peak in the north Tropical and Equatorial regions is lower. And the value shows thrice to fivefold as much as the Subtropical region. The latter peak may be caused by the upwelling of the subsurface water and also related to the California Current and Peru Current regions with very high concentration of nutrient matter. Because,

the observations by "Alise" (N/O Coriolis, 1957) which had a course along the equator show generally decrease of phosphate concentration in the surface and intermediate

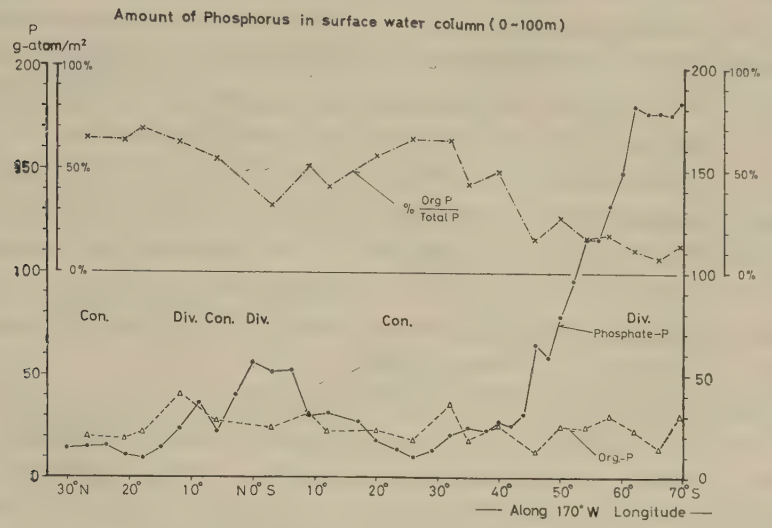

Fig. 5. Amount of phosphorus in surface water column (0-100 m).

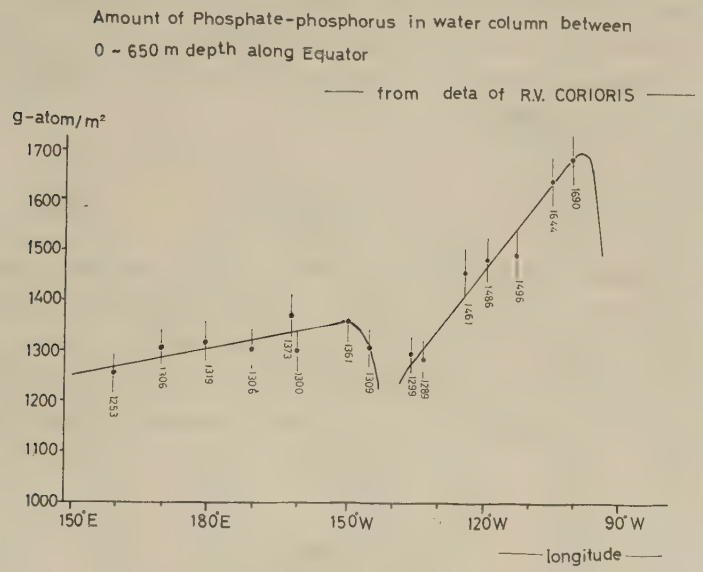

Fig. 6. Amount of phosphate-phosphorus in the water column between 0 and 650 m depth along the Equator.

waters to the west.

In Fig. 6, based on the data of "Alise" along the Equator, the total amounts of phosphate in the water column of 0–650 m depth were estimated. The phosphate concentration was homogeneous below the depth of about 600 m. The first peak which is shown around 100°W is related to the Peru Current area with high concentration of phosphate in the surface water and the second (near 150°W) again shows influences of above-mentioned area and upwelling from the subsurface.

The high concentration of nutrient in the surface water near the east coast of the Pacific is maintained by the upwelling of subsurface water. And those nutrients are transported westward by the trade wind in the Equatorial and Tropical regions reducing the concentration of nutrients. Such decrease of the concentration may be considered as the results of diffusion of water, the consumption by plankton and migration of organism to the deeper layers.

In the Subtropical regions along 170°W longitude, the amounts of phosphate in 0–100 m depth are generally small and the ratio of organic phosphorus to total phosphorus is more than 50% (see a chain line in Fig. 5). This superiority of organic phosphorus shows a tendency in which the biochemical balance between the production and breakup of organic matter inclines to the side of organic phosphorus owing to the poor nutrient in the environment.

The minima of the ratio of organic phosphorus to total phosphorus appear in the region of phosphate maxima. Moreover, the maxima and minima of the amounts of phosphate in the surface layer are closely related to the divergence area and convergence area respectively.

Acnowlegements

The author wishes to thank Prof. Y. MIYAKE for his kind encourangement and instraction. Tanks are also due to Prof. S. HORIBE for his kind guidance in the term of the observation, and Dr. Y. SUGIURA for the making of the report. Mr. T. FUJITA aided this work in the operation of analyses and Mr. T. YURA for the calculation of physico-chemical data. Mr. T. INOUE helped the constitution of the sentence.

References

HORIBE, Y. (editor) (1970): Preliminary report of the *Hakuho-Maru* cruise KH–68–4. Ocean

Research Institute of University of Tokyo.

KANAMORI, S. and T. SAKAMOTO (1968): Distribution de composants mineurs en océan profond—Principalement du bore et de l'arsenic—. *La mer*, **6**, 82–91, (in Japanese with French abstract).

MENZEL, D.W. and N. CORWIN (1965): The measurement of total phosphorus in sea water based on the liberation of organically bound fraction by persulfate oxidation. *Limnol. Oceanogr.*, **10**, 280–282.

Ocean Research Institute of University of Tokyo (1970): Oceanographic data of KH-68-4 (Southern cross cruise) of the *Hakuho-Maru*.

REDFIELD, A.C. (1960): The distribution of phosphorus in the deep ocean of the world. *Colect. Reprints, Woods Hole Oceanogr. Inst.*

REID, J.L.Jr. (1965): Intermediate waters of the Pacific Ocean. *Johns Hopkins Oceanographic Study*, **2**.

Resultates des observations physico-chemiques de la Croisiere "Alise" du N/O Coriolis ORSTOM centre de Nouméa (1967).

ROGER, C. (1967): Contribution à la connaisance des Euphausiaces du Pacifique Equatorial. *Cahier ORSTOM Serie Oceanographie*, **5** (1), 29–37.

SAPOZHNIKOV, V.V. and V.V. MAKIEVSKAYA (1966): Chemistry of the Pacific Ocean (BRUEVITCH, S.V., *et al.*). *Institution of Oceanography, USSR Academy Science*, 116–168, (in Russian).

STRICKLAD J.D.H. and T.R. PARSONS (1965): A manual of sea water analyses. *Fish. Res. Bd. Canada, Bull. No. 125*, 47–50.

SUGAWARA, K., M. AMBE, T. YOSHIHARA and S. YAMAGUCHI (1968): Progress reprot of the preparation of CSK standard chemical solutions, part 1, Phosphate-P standard solutions. Sagami Chemical Research Center.

YOSHIMURA, H. (1970): Distribution du phosphore dans eaux profondes du Pacifique—en relation avec la circulation profonde—. *La mer*, **8**, 19–26, (in Japanese with French abstract).

Results of Chemical Analyses

PO_4–P = Phosphate Phosphorus
ΣP = Total Phosphorus

KH-68-4. St. 4, Nov. 22, 1968 26°54′8N, 169°58′6W			KH-68-4. St. 11, Nov. 26–27, 1968 21°00′8N, 170°02′1W			KH-68-4. St. 13, Nov. 27–28, 1968 17°59′0N, 170°02′8W		
Depth (m)	PO_4–P (μg-atom/l)	ΣP (μg-atom/l)	Depth (m)	PO_4–P (μg-atom/l)	ΣP (μg-atom/l)	Depth (m)	PO_4–P (μg-atom/l)	ΣP (μg-atom/l)
0	0.14	0.28	0	0.07	0.30	0	0.15	0.35
8	0.11	0.21	10	0.14	0.28	9	0.13	0.32
24	0.15	0.33	28	0.16	0.29	27	0.12	0.35
40	0.25	0.34	47	0.07	0.26	44	0.10	0.32
59	0.00	0.38	70	0.01	0.32	66	0.00	0.31
79	0.17	0.39	94	0.22	0.34	87	0.18	0.32
116	0.26	0.48	140	0.23	0.36	129	0.07	0.32
152	0.29	0.54	187	0.33	0.40	170	0.19	0.41
226	0.49	0.69	281	0.72	0.86	253	0.62	0.78
300	0.87	1.03	376	1.62	1.66	336	1.69	1.67
375	1.10	1.28	472	2.34	2.47	419	2.13	2.38
451	1.32	1.73	566	2.88	2.89	502	2.69	2.92
530	1.69	2.28	661	3.06	3.17	589	2.86	3.05
610	2.39	2.68	754	3.18	3.17	677	2.98	3.12
774	2.88	3.19	943	3.05	3.17	859	3.06	3.12

946	3.05	3.42	952	2.84	3.25	1,051	2.91	3.12
1,074	2.85	3.34	1,140	3.14	3.25	1,296	2.96	3.12
1,342	3.05	3.19	1,223	3.21	3.18	1,566	2.91	3.08
2,256	2.67	3.15	1,682	3.05	3.15	2,010	2.68	2.90
2,707	2.68	3.05	2,144	3.07	2.95	2,463	2.68	2.90
3,161	2.57	2.93	2,588	2.75	2.85	3,358	2.48	2.68
3,625	2.49	2.53	3,042	2.67	2.91	3,810	2.28	2.80
			3,496	2.42	2.73	4,243	2.34	2.57
			3,938	2.34	2.75	4,700	2.68	2.59
			4,402	2.42	2.93	5,161	2.55	2.68

KH–68–4. St. 15, Nov. 29, 1968
11°59′7N, 169°49′5W

Depth (m)	PO_4–P (μg-atom/l)	ΣP (μg-atom/l)
0	0.23	1.16
9	0.18	0.72
26	0.22	0.48
43	0.22	0.87
64	0.21	0.48
85	0.17	0.48
127	0.68	1.12
170	1.45	1.67
255	2.35	2.68
342	2.56	2.82
429	2.62	3.03
519	2.71	3.25
609	2.98	3.25
700	3.03	3.34
888	3.06	3.36
1,080	2.93	3.28
648	2.71	3.16
931	3.15	3.28
1,412	2.77	3.15
1,900	2.71	3.05
2,377	2.77	2.90
2,850	2.81	3.05
3,326	2.43	2.86
3,801	2.46	2.71
4,276	2.39	2.72

KH–68–4. St. 17, Dec. 3, 1968
6°05′0N, 169°53′1W

Depth (m)	PO_4–P (μg-atom/l)	ΣP (μg-atom/l)
0	0.16	0.48
9	0.20	0.44
28	0.19	0.46
46	0.14	0.48
70	0.22	0.48
93	0.34	0.63
139	0.79	0.92
185	1.30	1.78
276	2.28	2.37
366	2.43	2.53
456	2.47	2.78
546	2.70	3.07
637	2.89	3.11
731	3.07	3.25
920	2.96	3.24
1,140	2.74	3.10
668	3.07	3.16
953	2.72	3.18
1,433	2.70	3.16
1,916	2.63	3.05
2,399	2.64	2.86
2,878	2.70	2.95
3,356	2.47	2.72
3,829	2.37	2.66
4,306	2.20	2.52
4,758	2.07	2.30
5,267	2.13	2.39

KH–68–4. St. 20, Dec. 6, 1968
3°01′9N, 170°01′6W

Depth (m)	PO_4–P (μg-atom/l)	ΣP (μg-atom/l)
0	0.48	0.72
9	0.49	0.72
28	0.50	0.76
47	0.51	0.78
71	0.50	0.76
95	0.59	0.81
142	0.76	1.01
189	1.26	1.51
284	1.81	2.03
379	2.47	2.51
474	2.52	2.68
569	2.65	2.84
667	2.82	2.99
761	2.95	3.10
953	2.90	—
1,148	2.83	3.08
1,031	2.74	3.17
1,319	2.94	3.05
1,796	2.77	3.09
2,275	2.69	3.03
2,750	2.62	2.74
3,226	2.66	2.86
3,703	2.54	2.70
4,178	2.38	2.39
4,654	2.32	2.68

KH–68–4. St. 22, Dec. 8, 1968
09°04′6S, 169°52′9W

Depth (m)	PO_4–P (μg-atom/l)	ΣP (μg-atom/l)
0	0.30	0.59
9	0.29	0.62
28	0.29	0.59
46	0.33	0.62
69	0.23	0.62
90	0.34	0.62
134	0.47	0.78
177	0.65	0.88

KH–68–4. St. 25, Dec. 16, 1968
19°59′7S, 170°03′2W

Depth (m)	PO_4–P (μg-atom/l)	ΣP (μg-atom/l)
0	0.25	0.45
10	0.17	0.41
29	0.20	0.45
48	0.22	0.38
73	0.12	0.41
97	0.20	0.45
144	0.11	0.36
190	0.28	0.39

KH–68–4. St. 29, Dec. 20–21, 1968
26°01′7S, 169°59′0W

Depth (m)	PO_4–P (μg-atom/l)	ΣP (μg-atom/l)
0	0.07	0.22
9	0.07	0.24
28	0.06	0.26
46	0.08	0.28
69	0.10	0.30
91	0.10	0.28
137	0.23	0.40
183	0.31	0.42

261	1.24	1.50	283	0.40	0.62	276	0.54	0.70
348	1.78	2.06	377	0.68	0.88	369	0.78	0.94
435	1.99	2.45	471	1.25	1.48	462	1.10	1.26
523	1.99	2.45	565	1.67	1.79	556	1.30	1.50
613	2.30	2.60	661	1.94	2.07	650	1.48	1.75
702	2.48	2.70	756	2.13	2.31	745	1.78	1.91
887	2.50	2.79	948	2.21	2.50	936	1.99	2.14
1,077	2.53	2.94	1,140	2.65	2.64	1,123	1.98	2.44
1,260	2.61	2.98	1,199	2.60	2.67	898	1.94	2.14
1,541	2.65	2.96	1,486	2.62	2.69	1,184	2.06	2.50
2,005	2.47	2.94	1,968	2.59	2.73	1,659	2.25	2.69
2,480	2.47	2.88	2,448	2.54	2.73	2,134	2.23	2.73
2,948	2.44	2.73	2,926	2.52	2.65	2,609	2.42	2.63
3,418	2.51	2.80	3,402	2.53	2.56	3,083	2.26	2.65
3,894	2.37	2.65	3,879	2.21	2.36	3,556	2.08	2.35
4,361	2.09	2.51	4,354	2.23	2.37	4,027	2.01	2.33
			4,828	2.05	2.30	4,492	2.06	2.29
			5,303	2.12	2.23	4,962	2.05	2.31
						5,441	2.00	2.19

KH-68-4. St. 31, Dec. 22-23, 1968
31°58′8S, 169°59′7W

Depth (m)	PO_4-P (μg-atom/l)	ΣP (μg-atom/l)
0	0.23	0.31
9	0.16	0.31
28	0.17	0.34
47	0.23	0.34
70	0.24	0.36
93	0.19	0.44
141	0.34	0.59
188	0.51	0.72
283	0.85	0.94
377	1.08	1.22
468	1.15	1.45
560	1.37	1.61
653	1.47	1.67
749	1.67	1.82
942	1.88	2.14
1,135	1.91	2.28
1,520	2.33	2.53
1,844	2.37	2.55
2,329	2.40	2.64
2,811	2.29	2.62
3,287	2.15	2.30
3,758	2.01	2.34
4,227	2.04	2.15
4,700	2.17	2.22
5,175	2.09	2.15
5,652	2.15	2.22

KH-68-4. St. 32, Dec. 23, 1968
35°00′0S, 169°59′1W

Depth (m)	PO_4-P (μg-atom/l)	ΣP (μg-atom/l)
0	0.30	0.53
9	0.27	0.41
28	0.24	0.39
47	0.23	0.38
71	0.24	0.38
94	0.15	0.49
141	0.44	0.68
188	0.78	0.88
282	0.96	1.05
375	1.09	1.28
469	1.22	1.52
563	1.49	1.62
657	1.44	1.70
752	1.72	1.82
941	1.91	2.09
1,136	2.09	2.24
1,129	2.16	2.28
1,415	2.26	2.50
1,890	2.34	2.59
2,365	2.26	2.57
2,839	2.32	2.60
3,310	2.09	2.41
3,778	2.02	2.23
4,246	2.09	2.34
4,715	2.10	2.30
5,198	2.10	2.28

KH-68-4. St. 34, Dec. 26, 1968
39°59′5S, 170°03′2W

Depth (m)	PO_4-P (μg-atom/l)	ΣP (μg-atom/l)
0	0.22	0.42
9	0.19	0.40
28	0.16	0.42
47	0.19	0.44
70	0.34	0.46
94	0.46	0.60
140	0.60	0.85
187	0.93	1.08
281	1.12	1.38
375	1.22	1.48
469	1.34	1.60
564	1.40	1.69
658	1.47	1.78
753	1.61	1.88
945	1.90	2.11
1,140	2.04	2.25
1,417	2.29	2.49
1,708	2.32	2.61
2,193	2.16	2.64
2,677	2.04	2.33
3,160	2.06	2.26
3,644	2.09	2.39
4,129	2.03	2.26
4,613	2.03	2.32

KH-68-4. St. 37, Dec. 28, 1968
46°01′3S, 169°58′6W

Depth (m)	PO_4-P (μg-atom/l)	ΣP (μg-atom/l)
0	0.54	0.67
9	0.57	0.67
27	0.54	0.67
45	0.58	0.72
67	0.79	0.88
90	0.73	0.84
135	0.57	0.88
181	0.99	0.95
273	1.17	1.28
366	1.12	1.37
459	1.31	1.53
552	1.44	1.55
645	1.36	1.61
738	1.58	1.71
927	1.96	1.94
1,120	2.00	2.15
1,047	1.97	2.12
1,348	2.06	2.38
1,834	2.11	2.49
2,320	2.15	2.48
2,806	2.05	2.11
3,289	2.12	2.26
3,769	2.05	2.20
4,249	2.05	2.22
4,730	2.13	2.18
5,209	2.16	2.18

KH-68-4. St. 39, Jan. 11, 1969
49°52′4S, 170°00′9W

Depth (m)	PO_4-P (μg-atom/l)	ΣP (μg-atom/l)
0	0.46	0.76
10	0.48	0.76
28	0.49	0.74
48	0.73	1.05
71	0.78	0.99
95	0.93	1.12
143	1.10	1.30
191	1.13	1.34
287	1.24	1.49
383	1.31	1.51
479	1.20	1.62
575	1.41	1.74
672	1.56	1.84
768	1.78	2.03
960	1.82	2.31
1,154	2.16	2.56
1,076	2.09	2.54
1,363	2.13	2.71
1,843	2.19	2.76
2,324	1.91	2.64
2,806	1.97	2.83
3,286	1.88	3.00
3,766	1.96	3.08
4,245	2.00	3.31
4,724	1.96	3.18
5,205	1.87	2.72

KH-68-4. St. 41, Jan. 12–13, 1969
53°58′2S, 169°55′6W

Depth (m)	PO_4-P (μg-atom/l)	ΣP (μg-atom/l)
0	0.99	1.24
9	1.06	1.24
28	0.92	1.24
46	1.10	1.43
69	1.26	1.49
91	1.35	1.49
137	1.42	1.53
184	1.37	1.53
276	1.54	1.66
368	1.72	1.84
459	1.76	2.00
550	1.80	2.20
639	2.06	2.34
727	2.19	2.38
905	1.94	2.50
1,088	2.34	2.58
1,097	2.26	2.50
1,386	2.27	2.49
1,869	2.11	2.34
2,349	1.94	2.18
2,829	1.98	2.39
3,309	2.14	2.49
3,787	2.04	2.48
4,263	2.06	2.48
4,739	1.98	2.49
5,214	1.94	—

KH-68-4. St. 43, Jan. 14–15, 1969
57°55′1S, 169°58′4W

Depth (m)	PO_4-P (μg-atom/l)	ΣP (μg-atom/l)
0	1.25	1.46
9	1.29	1.48
26	1.15	1.57
44	1.23	1.53
65	1.38	1.61
87	1.47	1.95
131	1.69	1.91
174	1.75	1.99
261	1.79	2.11
348	1.80	2.22
435	1.77	2.34
521	1.82	2.43
610	1.77	2.50
698	2.13	2.53
878	2.20	2.53
1,065	1.95	2.48
1,300	1.96	2.40
1,570	2.03	2.34
2,025	2.02	2.24
2,485	1.87	2.15

KH-68-4, St. 45, Jan. 16, 1969
61°58′9S, 169°57′6W

Depth (m)	PO_4-P (μg-atom/l)	ΣP (μg-atom/l)
0	1.62	1.70
8	1.53	1.79
26	1.41	1.87
42	1.75	2.06
63	2.06	2.10
84	2.02	2.23
125	2.15	2.28
166	2.28	2.36
250	2.38	2.45
334	2.42	2.53
419	2.18	2.48
505	2.26	2.46
593	2.34	2.44
681	2.20	2.41
863	2.17	2.34
1,056	2.23	2.30
1,154	1.96	2.30
1,434	2.02	2.28
1,914	2.10	2.28
2,407	2.02	2.22

KH-68-4. St. 47, Jan. 17, 1969
66°00′0S, 170°00′0W

Depth (m)	PO_4-P (μg-atom/l)	ΣP (μg-atom/l)
0	1.63	1.84
10	1.77	1.82
29	1.70	1.92
48	1.60	1.86
73	2.25	2.20
97	2.24	2.26
145	2.27	2.24
193	2.34	2.35
290	2.28	2.36
386	2.30	2.31
484	2.27	2.31
580	2.21	2.36
678	2.28	2.32
776	2.31	2.38
972	2.24	2.35
1,310	2.13	2.38
1,504	2.32	2.38
1,795	2.20	2.38
2,278	2.17	2.43
2,760	2.28	2.39

2,947	1.92	2.34	2,896	1.94	2.32	3,243	2.34	2.39
3,416	1.83	2.41	3,377	2.15	2.37			
3,886	1.95	2.38						
4,360	2.03	2.39						

KH-68-4. St. 49, Jan. 19, 1969
69°29′4S, 169°57′3W

Depth (m)	PO_4-P (μg-atom/l)	ΣP (μg-atom/l)
0	1.39	1.83
9	1.45	1.85
27	1.58	2.02
44	1.86	2.30
67	1.98	2.20
89	2.11	2.20
134	2.12	2.33
178	2.24	2.29
268	2.25	2.40
357	2.15	2.46
447	2.20	2.50
538	2.21	2.58
628	2.21	2.43
720	2.35	2.55
908	2.24	2.53
1,102	2.32	2.39
1,192	2.20	2.43
1,483	2.34	2.43
1,967	2.16	2.45
2,451	2.25	2.41
2,932	2.24	2.51
3,413	2.16	2.57
3,896	2.24	2.59
4,186	2.14	2.45

KH-68-4. St. 51, Jan. 21, 1969
66°30′0S, 170°08′0E

Depth (m)	PO_4-P (μg-atom/l)	ΣP (μg-atom/l)
0	1.93	2.04
10	1.84	—
29	1.94	2.23
49	2.02	2.22
97	2.07	2.40
195	2.36	2.46
392	2.23	2.40
590	2.20	2.42
788	2.42	2.54
986	2.34	2.45
1,185	2.33	2.43
1,691	2.34	2.43
2,172	2.09	2.49
2,656	2.31	2.54
3,141	2.34	2.68

KH-68-4. St. 52, Jan. 23-24, 1969
63°03′8S, 154°53′6E

Depth (m)	PO_4-P (μg-atom/l)	ΣP (μg-atom/l)
0	1.42	1.76
7	1.39	1.76
21	1.39	1.74
35	1.91	3.11
53	2.25	2.47
74	2.23	2.49
108	2.29	2.60
146	2.27	2.69
222	2.11	2.69
298	2.18	2.40
377	2.18	2.40
376	2.18	2.44
459	2.11	2.40
554	2.09	2.40
740	2.08	2.29
1,079	2.22	2.39
1,273	2.27	2.35
1,563	1.97	2.51
2,046	1.93	2.45
2,529	2.16	2.49
3,008	2.21	2.35

KH-68-4. St. 53, Jan. 24, 1969
60°00′3S, 155°02′5E

Depth (m)	PO_4-P (μg-atom/l)	ΣP (μg-atom/l)
0	1.29	1.17
10	1.43	—
29	1.58	2.00
49	2.06	2.28
97	2.27	2.41
194	2.45	2.61
386	2.15	2.50
578	2.08	2.40
771	2.02	2.41
965	2.04	2.41
1,159	2.19	2.39
1,217	2.24	—
1,504	2.14	2.37
1,983	2.04	2.53
2,467	2.12	2.51

KH-68-4. St. 54, Jan. 25, 1969
57°05′3S, 155°01′9E

Depth (m)	PO_4-P (μg-atom/l)	ΣP (μg-atom/l)
0	1.29	1.40
10	1.10	1.44
29	1.20	1.52
48	1.53	2.06
72	2.20	2.32
95	2.20	2.22
143	2.18	2.37
190	2.38	2.49
286	2.52	2.49
382	2.34	2.57
478	2.32	2.56
574	2.28	2.59
670	2.27	2.39
766	2.34	2.35
961	2.31	2.33

KH-68-4. St. 55, Jan. 26-27, 1969
53°56′9S, 155°08′0E

Depth (m)	PO_4-P (μg-atom/l)	ΣP (μg-atom/l)
0	1.23	1.48
9	1.29	1.48
28	1.31	1.46
47	1.10	1.50
71	1.55	1.69
95	1.52	1.77
142	1.53	1.81
190	1.55	1.86
285	1.56	2.02
381	1.87	2.20
477	1.86	2.28
573	1.93	2.38
669	2.06	2.46
765	2.10	2.56
959	2.24	2.63

2.958	2.23	2.57	1,158	2.11	2.18	1,153	2.14	2.71
			1,409	2.21	2.28	1,003	2.28	2.58
			1,696	2.27	2.32	1,292	2.35	2.53
			2,170	2.28	2.36	1,773	2.05	2.35
			2,648	2.11	2.16	2,254	2.04	2.32
			3,125	2.27	2.36	2,763	2.13	2.34
			3,606	2.26	2.41	3,215	2.16	2.45
						3,706	2.15	2.45

KH-68-4. St. 56, Jan. 27-28, 1969
51°10′4S, 155°23′9E

Depth (m)	PO_4-P (μg-atom/l)	ΣP (μg-atom/l)
0	0.84	0.98
10	0.79	0.99
28	0.80	0.99
47	0.79	0.98
71	0.88	1.02
95	0.98	1.06
142	1.17	1.23
189	1.16	1.27
284	1.20	1.31
380	1.18	1.31
485	1.22	1.39
581	1.25	1.39
676	1.43	1.55
771	1.82	1.84
961	2.08	2.14
1,155	2.18	2.33
1,339	2.40	2.52
1,630	2.34	2.47
2,107	2.10	2.28
2,583	2.01	2.18
3,059	2.17	2.22
3,534	2.18	2.34
4,009	2.13	2.28
4,487	2.08	2.32

KH-68-4. St. 57, Jan. 29, 1969
47°59′6S, 155°04′2E

Depth (m)	PO_4-P (μg-atom/l)	ΣP (μg-atom/l)
0	0.71	0.86
10	0.71	0.90
29	0.74	0.90
48	0.77	0.92
72	0.96	1.14
95	1.06	1.13
174	1.22	1.24
268	1.19	1.28
367	1.16	1.28
456	1.03	1.32
555	1.25	1.39
643	1.31	1.48
846	1.68	1.91
1,019	1.93	2.18
1,008	2.12	2.37
1,297	2.33	2.41
1,778	1.98	2.41
2,306	2.08	2.26
2,785	2.14	2.24
3,263	2.22	2.34
3,833	2.22	2.30
4,287	2.19	2.36

KH-68-4. St. 58, Jan. 29, 1969
46°54′9S, 155°02′9E

Depth (m)	PO_4-P (μg-atom/l)	ΣP (μg-atom/l)
0	0.46	0.80
10	0.66	0.81
29	0.64	0.81
49	0.75	1.08
73	0.86	1.12
97	0.72	1.04
146	1.01	1.06
195	1.07	1.14
293	1.17	1.25
391	1.22	1.31
489	1.14	1.34
587	1.23	1.40
686	1.39	1.64
784	1.59	1.86
982	1.87	2.14
1,180	2.20	2.35
1,518	2.10	2.41
1,803	2.21	2.40
2,284	2.13	2.24
2,766	2.01	2.19
3,245	2.00	2.26
3,721	2.18	2.64
4,196	2.14	2.47
4,670	2.05	2.26

KH-68-4. St. 59, Jan. 30, 1969
44°03′1S, 155°02′4E

Depth (m)	PO_4-P (μg-atom/l)	ΣP (μg-atom/l)
0	0.31	0.57
9	0.33	0.62
28	0.32	0.62
46	0.35	0.61
69	0.76	0.93
92	0.78	0.95
138	0.99	1.10
185	0.92	1.19
278	1.16	1.29
371	1.23	1.37
464	1.38	1.53
557	1.39	1.59

KH-68-4. St. 60, Jan. 31, 1969
41°01′8S, 155°02′3E

Depth (m)	PO_4-P (μg-atom/l)	ΣP (μg-atom/l)
0	0.22	0.56
9	0.20	0.46
28	0.19	0.54
46	0.23	0.52
69	0.41	0.66
92	0.53	0.78
138	0.76	0.91
184	0.79	1.09
275	1.01	1.20
366	1.16	1.35
455	1.20	1.49
545	1.34	1.57

KH-69-4. St. 61, Feb. 1, 1969
38°02′2S, 154°56′2E

Depth (m)	PO_4-P (μg-atom/l)	ΣP (μg-atom/l)
0	0.24	0.37
9	0.23	0.42
28	0.23	0.42
47	0.24	0.42
71	0.44	0.63
94	0.56	0.69
137	0.65	0.75
189	0.65	0.78
284	0.69	0.75
380	0.82	0.90
476	1.06	1.21
572	1.29	1.42

651	1.42	1.71	635	1.45	1.73	669	1.45	1.56
745	1.72	1.99	724	1.67	1.85	765	1.77	1.70
935	1.98	2.16	906	2.00	2.13	957	1.90	2.08
1,129	2.00	2.37	1,095	2.03	2.40	1,148	2.20	2.71
1,016	2.10	2.25	1,423	2.33	2.58	1,295	2.38	2.46
1,306	2.33	2.46	1,713	2.39	2.47	1,587	2.51	2.55
1,787	2.36	2.47	2,189	2.25	2.43	2,072	2.42	2.50
2,266	1.98	2.22	2,673	2.08	2.32	2,557	2.23	2.28
2,745	2.07	2.20	3,154	2.08	2.43	3,041	2.16	2.18
3,224	2.18	2.30	3,629	2.23	2.68	3,524	2.21	2.40
3,701	2.08	2.24	4,109	2.08	2.66	4,005	2.20	2.36
4,177	2.08	2.34	4,585	1.99	2.47	4,482	2.17	2.43
4,655	2.02	2.28						

170°W 線の太平洋および南極海のリンの分布

吉　村　広　三

（気象庁海洋気象部）

1968年の11月から1969年の3月にかけて行なわれた東京大学海洋研究所白鳳丸の南十字星航海のさい得られた 170°W 線および南極海周辺のリン酸塩および全リンの資料を検討し，下記の結論を得たのでとり合えず報告する．

1)　170°W 線に沿った断面図によれば，中層水および深層水中のリン酸塩は，ロス海を除き，北に向かうほど増加する．リン酸塩の極大層は亜南極海域から舌状に潜り込む中層水中の下部にあり，水温は 2～6°C，塩分は極少層の値（34～34.6‰）に近い．

2)　170°W の断面の有機体リンの分布について見ると，極大部とおぼしき海域が2箇所にあらわれている．すなわち，亜南極海域と赤道付近である．表層水のリンも南極海域と赤道付近に極大があり，前者のほうが著しく大きい．

3)　亜熱帯および熱帯海域の表層水中では，全リン中に占める有機体リンの比率が著しく高い．このことは光，水温などがプランクトンの繁殖に適しているためと考えられ，無機リンは殆んど消費されている．

なお，使用した分析法はリン塩酸については塩化第一錫を還元剤としたリン・モリブデン酸法，全リンについてはアスコルビン酸で還元したリン・モリブデン酸法を使用した．有機体中のリン酸の解離には Menzel による過硫酸カリウム分解法を使用した．アスコルビン酸還元のさい問題となるケイ酸塩の影響は測定結果から差し引いた．また同一発色のため妨害となるヒ素の影響も有機体リンの算出に当っては考慮した．

昭和47年12月27日　発行

編集兼発行者　気象庁
東京都千代田区大手町1の3の4

印刷者　藤原秀雄

印刷所　昌美印刷株式会社
東京都千代田区神田錦町3の16